The Dynamics of Error Processing in the Human Brain as Reflected by High-Gamma Activity in Noninvasive and Intracranial EEG

Abbreviated title: High-Gamma Activity in Human Error Processing

Martin Völker[1,2,3,4], Lukas D.J. Fiederer[1,4,5,6]*, Sofie Berberich[1,7]*, Jiří Hammer[1,4,8]*, Joos Behncke[1,3,4], Pavel Kršek[8], Martin Tomášek[8], Petr Marusič[8], Peter C. Reinacher[7,9], Volker A. Coenen[7,9], Moritz Helias[10], Andreas Schulze-Bonhage[4,7,11], Wolfram Burgard[3,4,12] and Tonio Ball[1,4,6,7]

1 - Translational Neurotechnology Lab, Medical Center – University of Freiburg, 79106 Freiburg, Germany
2 - Graduate School of Robotics, University of Freiburg, 79106 Freiburg, Germany
3 - Department of Computer Science, University of Freiburg, 79110 Freiburg, Germany
4 - BrainLinks-BrainTools, University of Freiburg, 79110 Freiburg, Germany
5 - Faculty of Biology, University of Freiburg, 79104 Freiburg, Germany
6 - Bernstein Center, University of Freiburg, 79104 Freiburg, Germany
7 - Faculty of Medicine, University of Freiburg, 79106 Freiburg, Germany
8 - Charles University, Second Faculty of Medicine, Motol University Hospital, 15006 Prague, Czech Republic
9- Stereotactic and Functional Neurosurgery, Medical Center – University of Freiburg, 79106 Freiburg, Germany
10- Institute of Neuroscience and Medicine (INM-6) and Institute for Advanced Simulation (IAS-6), Jülich Research Centre and JARA, 52428 Jülich, Germany
11 - Epilepsy Center, Medical Center – University of Freiburg, 79106 Freiburg, Germany
12 - Autonomous Intelligent Systems, University of Freiburg, 79110 Freiburg, Germany
* These authors contributed equally to this work.

Corresponding author: Martin Völker, Translational Neurotechnology Lab, Engelbergerstr. 21, 79106 Freiburg, Germany, email martin.voelker@uniklinik-freiburg.de

Number of pages: 48

Number of figures: 12

Number of tables: 2

Number of words in Abstract: 246

Number of words in Introduction: 654

Number of words in Discussion: 2378

Conflict of Interest: The authors declare no competing financial interests.

Abstract

Error detection in motor behavior is a fundamental cognitive function heavily relying on cortical information processing. Neural activity in the high-gamma frequency band (HGB) closely reflects such local cortical processing, but little is known about its role in error processing, particularly in the healthy human brain. Here we characterize the error-related response of the human brain based on data obtained with noninvasive EEG optimized for HGB mapping in 31 healthy subjects (15 females, 16 males), and additional intracranial EEG data from 9 epilepsy patients (4 females, 5 males). Our findings reveal a comprehensive picture of the global and local dynamics of error-related HGB activity in the human brain. On the global level as reflected in the noninvasive EEG, the error-related response started with an early component dominated by anterior brain regions, followed by a shift to parietal regions, and a subsequent phase characterized by sustained parietal HGB activity. This phase lasted for more than 1 s after the error onset. On the local level reflected in the intracranial EEG, a cascade of both transient and sustained error-related responses involved an even more extended network, spanning beyond frontal and parietal regions to the insula and the hippocampus. HGB mapping appeared especially well suited to investigate late, sustained components of the error response, possibly linked to downstream functional stages such as error-related learning and behavioral adaptation. Our findings establish the basic spatio-temporal properties of HGB activity as a neural correlate of error processing, complementing traditional error-related potential studies.

Significance Statement

There is great interest to understand how the human brain reacts to errors in goal-directed behavior. An important index of cortical and subcortical information processing is fast oscillatory brain activity, particularly in the high-gamma band (above 50 Hz). Here we show that it is possible to detect signatures of errors in event-related high-gamma responses with noninvasive techniques, characterize these responses comprehensively, and validate the EEG procedure for the detection of such signals. In addition, we demonstrate the added value of intracranial recordings pinpointing the fine-grained spatio-temporal patterns in error-related brain networks. We anticipate that the optimized noninvasive EEG techniques as described here will be helpful in many areas of cognitive neuroscience where fast oscillatory brain activity is of interest.

Introduction

Error processing is a fundamental brain function. A breakthrough in research on error processing in the human brain was the independent discovery of the "error-related negativity" (ERN) (Gehring et al., 1993), or error negativity (Ne) (Falkenstein et al., 1991) in noninvasive electroencephalography (EEG). The ERN/Ne is a negative deflection above the fronto-central midline, peaking shortly after the electromyogram (EMG) onset of an erroneous response, followed by the error positivity (Pe) (Falkenstein et al., 1991) with parietal maximum. ERN/Ne and Pe are often assumed to reflect sequential functional aspects of error processing, including precursors of error detection such as conflict monitoring and explicit error detection itself. In contrast to the ERN/Ne, the Pe was linked to conscious error processing (Nieuwenhuis et al., 2001). Moreover, the Pe

3

77   might reflect evidence strength during error detection and could thus provide input to

78   further downstream stages, e.g., to the evaluation of the significance of errors and the

79   implementation of behavioral reactions (Steinhauser and Yeung, 2010).

80   To further dissect error-related processing both in healthy subjects and in patients with a

81   broad spectrum of brain disorders (Alain et al., 2002; Hajcak et al., 2003; Shiels and

82   Hawk, 2010), subsequent studies increasingly utilized time-frequency decomposition of

83   error-related EEG responses. These studies revealed spatial and dynamical behavior of

84   lower frequency bands like delta, theta, alpha and beta (Table 2) unfolding alongside the

85   time-domain (ERN/Ne & Pe) evoked electrical field potential changes. There is only

86   limited data on the role of higher frequencies in error processing, coming from

87   intracranial recordings in neurological patients (Milekovic et al., 2013; Bastin et al., 2017)

88   and we are not aware of any other study using noninvasive EEG recorded from the

89   healthy human brain.

90   However, gamma-band frequencies may be especially important to understand cortical

91   function in general, including error processing. A large body of empirical evidence

92   indicates that high-gamma band (HGB, including the 50-150 Hz range) activity is a

93   spatially and temporally specific index of the underlying, functionally relevant neural

94   networks (Crone et al., 1998, 2006; Brunel and Wang, 2003). Compared to lower

95   frequencies, however, detecting HGB power modulations in noninvasive EEG is

96   challenging for several reasons that are related to the more focal spatial distribution of

97   cortical high-frequency sources (Crone et al., 2006), their much smaller power,

98   (Freeman et al., 2000), and their greater susceptibility to artifacts, such as from muscle

99   activity (Goncharova et al., 2003) or microsaccades. The latter particularly can mimic

100   physiological responses within the HGB range (Yuval-Greenberg et al., 2008).

101   To overcome these problems, we carefully optimized the procedure of EEG acquisition

102   and analysis for the detection of high-frequency EEG modulations, combining high-

103   resolution EEG acquisition, optimized electromagnetic shielding, low-noise amplifier

104   systems, as well as high-precision eye tracking simultaneously acquired to the EEG data

105   to tightly control for ocular artifacts. Utilizing this optimized setup, we re-examined a

106   classical paradigm to elicit error responses in a large group (n=35) of healthy subjects.

107   Furthermore, to validate our noninvasive EEG findings, we also ran the same paradigm

108   in patients with intracranially implanted electrodes.

109   Our findings clearly demonstrate that error-related HGB brain responses can be

110   detected in noninvasive EEG recorded from healthy subjects; importantly, we rule out

111   ocular including micro-saccadic effects as an explanation for the observed HGB

112   responses, as well as corroborate our noninvasive observations by intracranial EEG

113   data. For the first time, our findings reveal a clear picture of the global dynamics of the

114   error-related HGB response of the human brain, starting from an early response

115   dominated by anterior brain regions, over a shift to medial parietal regions parallel to the

116   Pe, and finally to a subsequent phase characterized by sustained parietal HGB activity.

117   This phase lasts for more than 1 s after the onset of the error event and constitutes a

118   novel candidate signal of the downstream processes following the classical Pe.

119   Combined investigation of both the classical error-related potentials and of HGB

120   modulations thus promises to shed new light on error processing in the human brain.

5

Materials & Methods

Subjects

In the noninvasive EEG study, 35 healthy subjects participated; thereof, 4 subjects had to be excluded because of extensive muscular or ocular artifacts. Thus, data of 31 subjects (mean age 24.6 years, standard deviation (SD) = 3.1 years, 15 females) were further analyzed. Handedness was assessed according to a modified Edinburgh handedness questionnaire (Oldfield, 1971); 28 subjects were right-handed, 3 were left-handed. All stated not to have neurological or psychiatric diseases and not to be under the influence of medication affecting the central nervous system.

In the intracranial EEG study, 9 right-handed patients (mean age 27.0 years, SD = 7.7 years, 4 females) with pharmacoresistant epilepsy were recruited. They were implanted with intracranial electrodes in Freiburg, Germany, or in Prague, Czech Republic.

All subjects and patients gave their written informed consent before participating in the study. The study was approved by the local ethics committees.

Experimental design

To probe error-related processing, we used the Eriksen flanker task (Eriksen and Eriksen, 1979) (Fig. 1) as employed in a pioneering study in this field of research (Gehring et al., 1993) as well as in many follow-up publications (Kopp et al., 1996; Botvinick et al., 1999; Gehring and Knight, 2000; Nieuwenhuis et al., 2002; Ridderinkhof et al., 2002; Herrmann et al., 2004b; Albrecht et al., 2009; Maier et al., 2012; Zavala et al., 2013). At the beginning of each trial, a cue in the form of an asterisk was shown to the subjects in the center of a 19-inch monitor (4:3-screen ratio, 60-Hz frame rate) for

143   1 s. After that, one of four stimuli was shown for 100 ms, each with a probability of 0.25.

144   Two of the stimuli were *congruent stimuli* (LLLLL & RRRRR) and the other two

145   *incongruent stimuli* (RRLRR & LLRLL). To respond, subjects used their left or right

146   index finger to press the left or right analog shoulder button on a wireless gamepad

147   (Logitech F710, Apples, Switzerland) if the central letter of the stimulus was an "L" or

148   "R", respectively. The deflection threshold of the analog joystick button was set to 10%

149   of its maximal deflection.

150   As proposed by (Herrmann et al., 2004b), we set an individual reaction time limit for

151   each subject. This response time limit was determined as the mean response time in a

152   32-trial training session. Subjects were instructed to respond as fast and as accurately

153   as possible. The subjects were also introduced to a scoring point system, and instructed

154   to get as many points as possible. For each correct response, subjects gained 5 points,

155   and lost 5 points in the event of an erroneous response. By missing the individual

156   reaction time limit, subjects lost 10 points; this stronger penalty was introduced to keep

157   the subject under time pressure, hence inducing errors. In each break after a recording

158   run, the score and performance of the respective run was shown to the subjects along

159   with a comparison to their total performance up to this run.

160   Two seconds after their response, the subjects received an audiovisual feedback

161   according to their performance. If the response was fast enough and correct, the

162   feedback consisted of a smiling face icon and a 1-kHz sine tone, the feedback for an

163   erroneous but fast enough response consisted of a sad face and a 500-Hz sine tone.

164   For responses slower than the individual reaction time limit, a cartoon of a snail was

165   displayed accompanied by a 5-kHz sine tone. The two-second delay was introduced to

7

166   avoid an influence of the feedback on error-related brain responses. We did not verify

167   the error awareness prior to the feedback directly; however, all subjects reported that

168   they were aware of most errors directly after the motor response.

169   Before the start of each trial, only the fixation dot was shown for 3 s. In the case of

170   healthy subjects, one session consisted of 100 trials, after which the subjects had the

171   possibility to have a break. Each experiment included 10 sessions, so that altogether

172   1000 trials were collected for each subject; on average, the error rate was 22.23 ± 0.11

173   (mean ± SD) %. Recording sessions with epilepsy patients were shorter and included

174   overall fewer trials depending on the condition of the respective patient. On average,

175   patients completed 369 ± 111 trials, thereof 218 ± 74 correct trials and 57 ± 32 error

176   trials, with a total error rate of 20.95 ± 0.11 %.
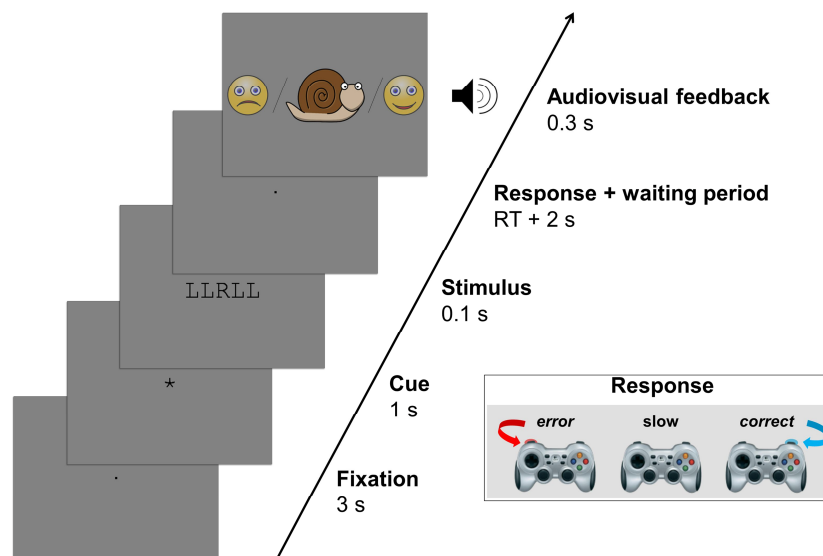
177

178   **Figure 1: Flowchart of the Eriksen flanker task paradigm used to elicit errors.**

179   After a fixation period (3 s), and a cue period (1 s), the stimulus appeared for a short period of time

180   (100 ms). Subjects had only a limited amount of time, individually set to their reaction time (RT) in a

181   familiarization phase of the experiment, to press a gamepad button with their left index finger if the central

182   letter of the stimulus was an "L" or with their right index finger if the central letter was an "R" (see example

8

183 with 'R' target letter in inset). 2 s after the button press, one of the three types of audiovisual feedback

184 indicated to the subjects whether their response was correct, incorrect, or too slow.

Recording and preprocessing of noninvasive EEG

186 The noninvasive EEG setup was optimized for the measurement of high-frequency

187 responses. We used NeurOne amplifiers (Mega Electronics Ltd., Kuopio, Finland) with a

188 24-bit resolution and low input noise (root mean square < 0.6 µV between 0.16-200 Hz).

189 We recorded 128 EEG channels with the waveguard EEG cap (ANT Neuro, Enschede,

190 Netherlands) at a sampling rate of 5 kHz (AC, 1250-Hz anti-aliasing low-pass filter). The

191 cap held sintered Ag/AgCl electrode elements and was available in three different sizes

192 to be suitable for variable head sizes. Electrode position Cz was used as recording

193 reference; the ground was located between AFz and Fz. Whenever possible,

194 impedances were kept below 5 kΩ. Additional measurements included

195 electrooculography (EOG) with 4 electrodes around the eyes, 2-channel

196 electrocardiography (ECG) and bipolar electromyography (EMG) above the forearm

197 flexor muscles of both arms and above the gastrocnemius muscle of both legs; EMG,

198 EOG and ECG were recorded with self-adhesive electrodes.

199 The EEG recordings took place in an electromagnetically shielded cabin ("mrShield" -

200 CFW Trading Ltd, Heiden, Switzerland) to reduce electromagnetic artifact

201 contamination. All exchange of information between inside and outside of the cabin was

202 done with fiber optic cables to sustain the shielding. Also, electrical devices inside the

203 cabin, such as EEG amplifier, eye tracker and loudspeakers, were powered by DC

204 batteries to prevent 50-Hz power line artifacts from interfering with the EEG signal. The

205 cabin furthermore dampens sounds and vibrations to protect the subject from external

206   noise.

207   Both control of the experiment as well as data analysis was carried out using Matlab

208   R2014a (The MathWorks Inc., Natick, USA, RRID:SCR_001622). Implementation of the

209   paradigm was done within the Psychophysics Toolbox (Brainard, 1997,

210   RRID:SCR_002881). Synchronization of the EEG data and the experimental paradigm

211   was achieved by using a parallel port to send different trigger pulses for each event from

212   Matlab to the EEG amplifiers.

213   To control the signal quality, a visual inspection of the EEG data was done both

214   continuously during the measurement as well as after the experiment in Brainstorm

215   (Tadel et al., 2011). We searched for EMG artifacts by examining time course and

216   topography of single-trial data. Channels with strong contamination with EMG artifacts

217   were excluded from further analysis in single subjects; on average, we rejected 1.03 ±

218   1.75 (mean ± SD) channels.

219   During signal processing, the EEG data and markers were down-sampled from 5 kHz to

220   1 kHz (time-frequency analysis) or 500 Hz (voltage plots). Channels were re-referenced

221   to their common average. The signal was filtered with a Butterworth high-pass filter of

222   fourth order with a cut-off frequency of 0.5 Hz.

223   The indices of the correct and false responses were extracted and aligned on the

224   response EMG. The time point of the EMG onset was found by applying a threshold

225   based retrospective search on the arm EMG channels.

226   **Intracranial EEG recording, localization and preprocessing**

227   Recording of intracranial EEG signal was done either with Compumedics amplifiers

228   (Singen, Germany) at the epilepsy center in Freiburg, Germany (2 kHz sampling rate), or

229   with Schwarzer Epas amplifiers (Munich, Germany) and Nicolet EEG C-series amplifiers

230   (Pleasanton, USA) at the epilepsy center of the Motol University Hospital in Prague,

231   Czech Republic (512 Hz sampling rate). The depth electrodes used for recording had

232   platinum-iridium contacts (DIXI Medical, Lyon, France & AD-TECH, Racine, WI, USA).

233   The preprocessing was done as for the noninvasive data, with the difference that the

234   channels were re-referenced bipolarly between the respective neighbors.

235   The stereotactic depth electrodes were localized with the help of their post-implantation

236   MRI or CT artifacts in a normalized and co-registered MRI of each patient as described

237   in Pistohl et al. (2012). After transformation to the MNI coordinate system,

238   cytoarchitectonic probabilistic maps were calculated with the SPM anatomy toolbox

239   (Eickhoff et al., 2005, 2006, 2007) to assign the electrodes to specific brain regions. This

240   method accounts for inter-subject differences in brain anatomy and allows the

241   comparison on a group level with high precision (Amunts et al., 2007).

242   Electrodes positioned inside a seizure onset zone or showing frequent interictal activity,

243   as identified by experienced epileptologists, were excluded from further analysis. Of 885

244   bipolar referenced channels from 9 patients, we removed 76 channels because they

245   could not be assigned to a specific brain region, 53 channels which were positioned

246   inside a seizure onset zone, 59 channels because of frequent interictal activity, and 7

247   channels due to technical problems or position outside the brain. Approximately 20 % of

248   the remaining electrodes were identified as lying within white matter. As a control, we

249   also did the analyses of the intracranial data after splitting white and gray matter

250   electrodes; however, as we found that white matter electrodes, especially those near

11

251   boundary areas, were able to sample a number of significant effects, and further did not

252   change any findings, we did not exclude these channels from further analysis.

253   Thus, 690 sites were available for further analysis.

254   The visualization of intracranial and scalp EEG electrodes in relation to the cortex

255   surface was done with Brainstorm (Tadel et al., 2011). The intracranial electrodes were

256   visualized on an ICBM152 brain template (Mazziotta et al., 2001; Fonov et al., 2009).

257   **Time-frequency analysis**

258   Time-resolved spectral power was computed with a multitaper method (Thomson, 1982)

259   with a window length of 500 ms, a step size of 50 ms and two Slepian taper functions.

260   Trial averages were computed with a median function, which proved to be a robust

261   method in past EEG studies (Ball et al., 2008). To visualize error-related power

262   modulations we baselined all time-frequency bins in each error trial by the corresponding

263   bin of the median correct response trial (i.e., by dividing the error responses by median

264   of the correct responses). Thus, the motor-related activity common to both response

265   types canceled out. For calculation of error-related activity or power, this method of

266   baselining was applied.

267   **Exclusion and statistical matching of ocular artifacts**

268   Ocular movements were recorded with the EyeLink 1000 plus (SR Research Ltd.,

269   Ottawa, Canada, RRID:SCR_009602), enabling binocular eye movement recordings

270   with a high-speed infrared illuminator and camera; the sampling rate for binocular

271   recording was 500 Hz.

272   For the extraction of microsaccades, an algorithm as described by Engbert and Kliegl

273 (2003) was used with the default minimal microsaccade duration threshold of 12 ms.

274 Time points of blinks and saccades were identified with the algorithms provided by the

275 EyeLink recording software.

276 All trials in which a blink occurred within the time window of 0.5 s prior and 2 s after the

277 response were excluded from further analysis to ensure that the EEG signal in the

278 analyzed time frame was not contaminated with blink artifacts. On average, 112 ± 164

279 (mean ± SD) trials were rejected across subjects.

280 To exclude possible influences of saccades and microsaccades on high-frequency EEG

281 correlates, we matched each time bin of the correct and error trials after the time

282 frequency decomposition. This was done by incrementally removing time bins from the

283 correct condition, which always had more trials. At each iteration step, the time bin which

284 contributed the most to the residual difference, as calculated by a sum of squares of

285 saccade and microsaccade counts, was removed. This process was repeated until the

286 p-value calculated with a sign test comparing error and correct condition was greater

287 than 0.3.

288 **Statistical analysis**

289 For visualization of median voltage, the standard error of the median was calculated per

290 condition using bootstrap sampling (Moore and McCabe, 1989) with 1000 re-samples,

291 using the 2.5^{th} and 97.5^{th} percentile of the population as standard error. Median time or

292 frequency bins which had a significant difference between the correct and erroneous

293 condition were identified with the Wilcoxon rank sum test (Mann and Whitney, 1947) in

294 single subjects or with a two-sided sign test (Dixon and Mood, 1946) across subjects.

295 Significance of median power changes within individual conditions was computed with a

13

296   two-sided sign test. Whenever multiple comparisons were done, we estimated the

297   positive false discovery rate (pFDR) for each p-value (Benjamini and Hochberg, 1995;

298   Storey, 2002, 2003).

Results

300   Here we show for the first-time error-related high-gamma responses in a noninvasive

301   EEG study (with 31 healthy subjects) and additionally compare and corroborate them

302   with intracranial EEG measurements (in 9 patients with pharmacoresistant epilepsy).

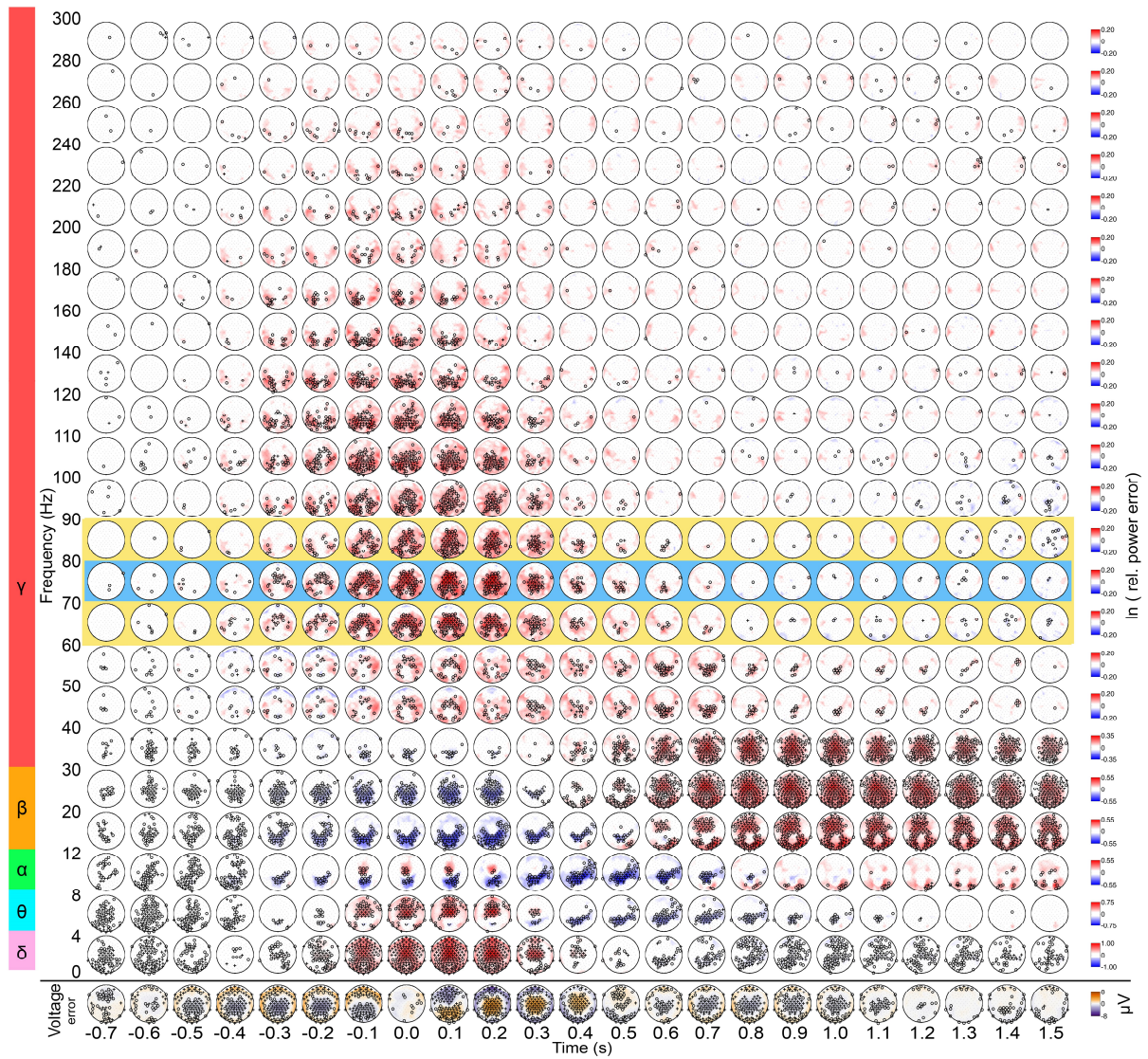### Error-related voltage and spectral power modulations in noninvasive EEG

304   In the following, we show an overview of the dynamics and topography of voltage and

305   spectral power modulations, as averaged over the 31 healthy subjects included in this

306   study, in correct responses (Fig. 2), erroneous responses (Fig. 3) as well as the

307   difference between the two conditions, i.e., error-related activity (Fig. 4). The spectral

308   power responses are shown up to 300 Hz in the time interval from 0.7 s before until 1.5

309   s after the response. For these and all comparable topographical results, the positive

310   false discovery rate was calculated across 128 channels, 24 frequency bands, and 61

311   time points (1 s before response onset until 2 s after response onset in steps of 50 ms).

312   Error-related HGB activity had its maximum approximately between 60 and 90 Hz (Fig.

313   2-4, yellow background), or more narrowly located between 70 and 80 Hz (Fig. 2-4, blue

314   background). Based on these observations, we decided to use these frequency ranges

315   for a closer inspection of HGB responses in the following analyses

14
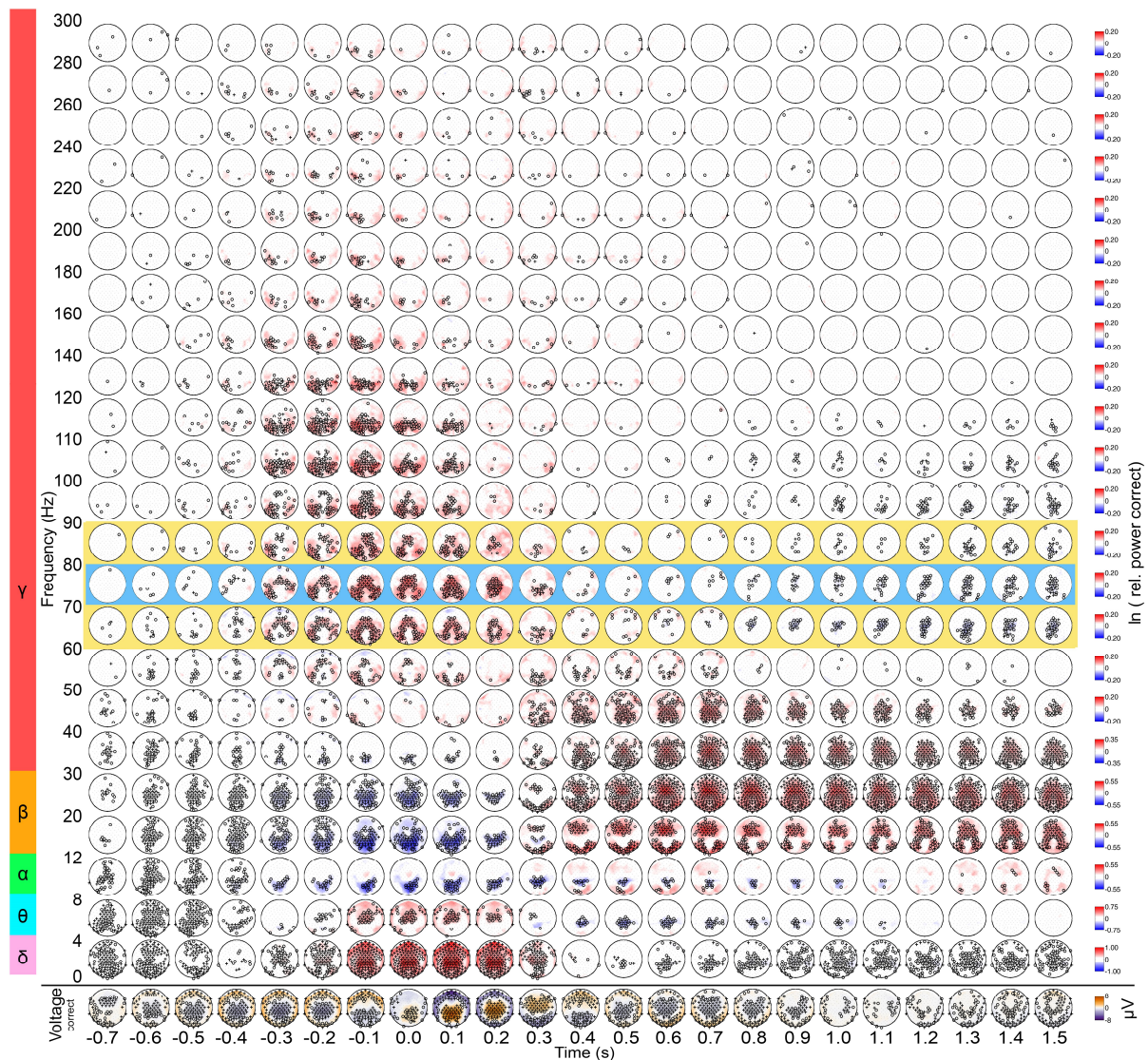
Figure 2: Topography of voltage and spectral power modulations in a correct response.

The circular plots represent a top view of the head with the nose pointing up. At the bottom, the average response is plotted (median of 31 subjects). Above, the median spectral power modulations relative to the time from -1 s to -0.5 s prior to the response, are depicted for 23 frequency bands from 0 to 300 Hz. Red color indicates higher power than in the baseline, blue color indicates lower power than in the baseline period. Electrodes with significant power modulations are marked with "o" or "+" (sign test, pFDR<0.05 or pFDR<0.01, respectively). The data is aligned to response onset.

15

Figure 3: Topography of voltage and spectral power modulations in an error response.

All conventions as in Figure 2.

16
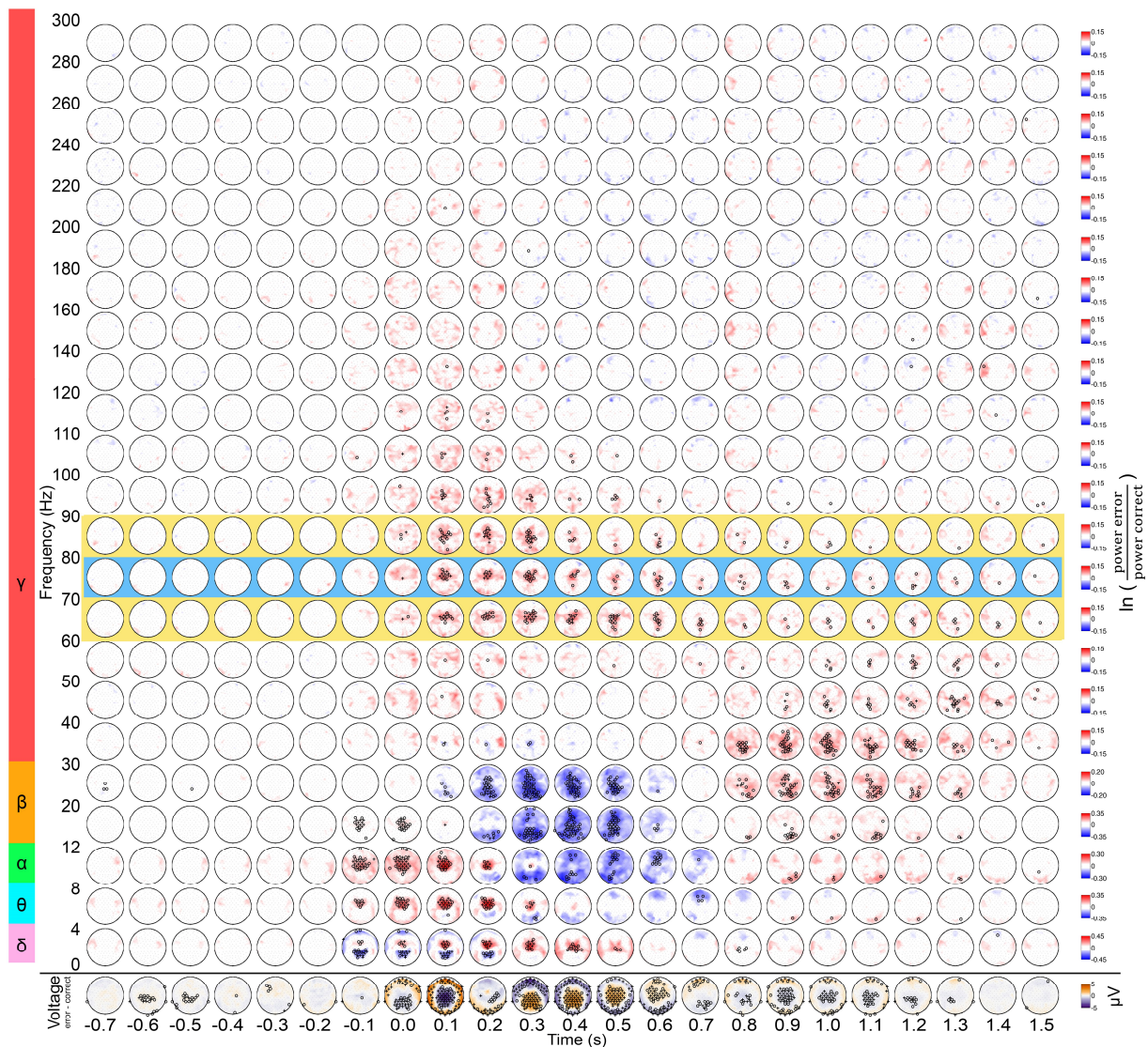
Figure 4: Topography of error-related voltage and spectral power modulations.

Conventions as in Figure 2. At the bottom, voltage differences between error and correct response are shown topographically (median of 31 subjects). Above, median error-related spectral power modulations are shown, i.e., each time-frequency point of the error response was baselined with the same point of the median correct response. Red color indicates higher power in error responses, while blue color indicates higher power in correct responses. Electrodes with significant differences between error and correct condition are marked with "o" or "+" (sign test, pFDR<0.05 or pFDR<0.01, respectively). The data is aligned to response onset.

17

336 Comparing error and correct conditions, significant differences became evident. While

337 there was lower power at parietal channels in the delta band (< 4 Hz) during and after

338 errors, fronto-central channels exhibited an error-related power increase in the delta and

339 the theta band (4-8 Hz). In the alpha band (8-12 Hz), a spatially more widespread power

340 increase during and shortly after the erroneous response occurred, followed by an

341 attenuation with lower power compared to correct responses. Within the beta band (12-

342 30 Hz), a widespread power decrease concurred with the Pe. In the low-gamma band

343 (LGB, 30-50 Hz), differences were mostly apparent at a later time, starting 800 ms post-

344 response in the form of a power increase in the 30-40 Hz frequency range.

345 Simultaneously with the late LGB increase, a second (with the ERN/Ne being the first)

346 significant negative voltage deflection was seen at central channels.

347 Crucial to the present study, in the high-gamma band (HGB, > 50 Hz), a significant

348 error-related power increase occurred at fronto-central channels shortly after the

349 response onset, and shifted to more central and parietal areas over the course of a few

350 hundred milliseconds, where the error-vs-correct relative HGB power stayed significantly

351 increased until up to 1.5 s after the response. Similar high-gamma increases were

352 observed in errors both after incongruent and congruent stimuli classes (data not

353 shown). After an initial HGB power increase, there was a significant midline power

354 decrease in correct responses after 800 ms until at least 1.5 s (Fig. 2). This power

355 decrease was not observed after erroneous response (Fig. 3)

356 Fig. 5 depicts the median frequency profile of the correct, error and error/correct

357 conditions for a central region of interest (ROI).

18
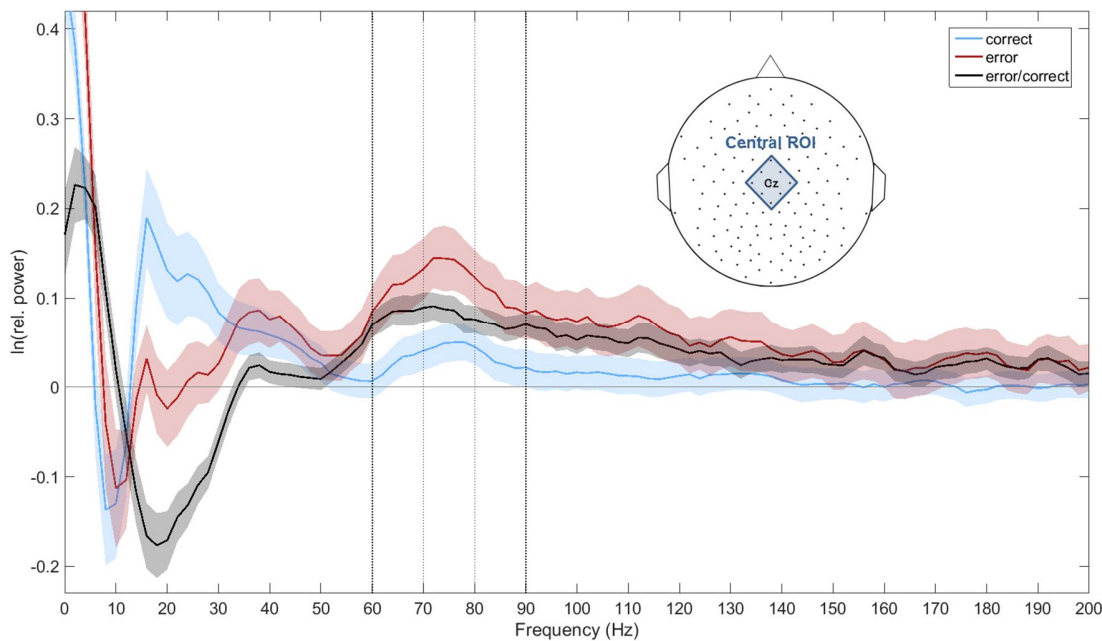
Figure 5: Frequency profile of spectral power modulations in an Eriksen flanker task.

The average frequency profile for the correct (blue), error (red) and error/correct condition (black) is shown averaged over a central ROI (FCz, FCC1h, FCC2h, C1, Cz, C2, CCP1h, CCP2h, CPz) during a time of interest between 0 s and 0.6 s relative to response onset. The SEM is plotted semitransparent. While relative power changes were highest in the delta (0-4 Hz) and theta (4-8 Hz) range, strong modulations were also observed in the alpha (8-12 Hz), beta (12-30 Hz) and high-gamma (> 50 Hz) range. The two frequency ranges of interest in the high-gamma range are marked with bold (60 to 90 Hz) and thin (70 to 80 Hz) dashed lines, respectively.

Error-related voltage and spectral power modulations of selected frequency bands in surface EEG are shown in Fig. 6. Topography and time course of the classical ERN/Ne and Pe components can be seen in the upper part. In the lower part of the figure, the relative power differences between error and correct condition are plotted in five frequency ranges of interest at the time point of the ERN/Ne and Pe components.

19
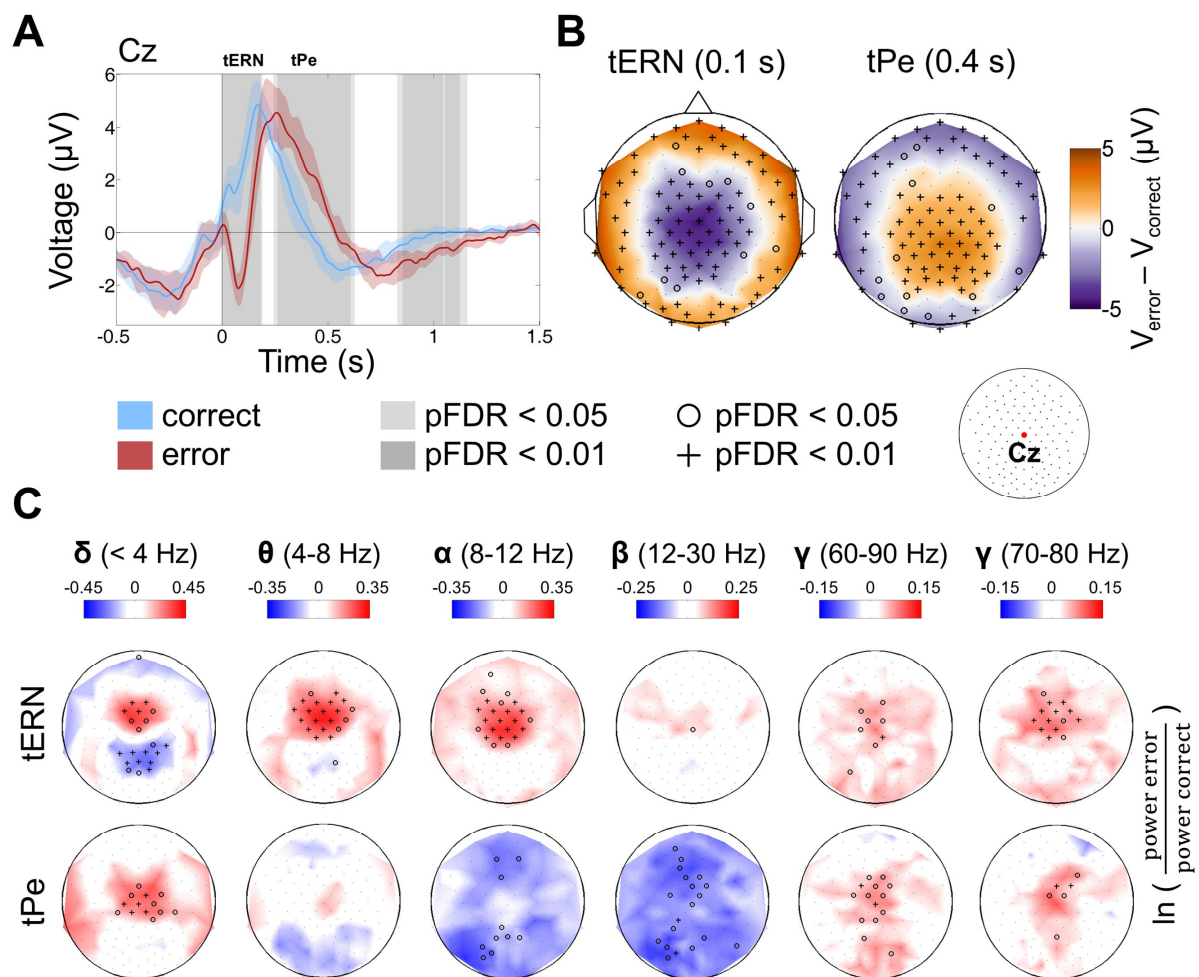
Figure 6: Error-related voltage and spectral power modulations in high-density EEG.

A) Single channel plot (electrode position Cz) locked to response EMG onset. The median correct response is shown in blue, the median erroneous response in red. The standard error of the median is plotted semitransparent. The vertical dotted line marks the EMG onset. Times with significant differences between the error and correct condition are shown with a gray background; pFDR values were calculated across 1501 time points (-1 s to 2 s, 500 Hz). **B)** Topographical map of the event-related potentials at the time of the ERN/Ne (t_{ERN}) and the Pe (t_{Pe}) components. Median voltage difference between error and correct trials is shown color coded. Electrodes with significant differences are marked with "o" or "+" (sign test, pFDR<0.05 or pFDR<0.01, respectively); pFDR values were calculated across 31 time points (-1 s to 2 s in steps of 100 ms) and 128 channels. **C)** Error-related spectral power modulations in the theta, alpha, beta, and high-gamma range. Logarithmic relative power of the median erroneous response baselined

20

384   with median correct response is shown color coded. Significant sites as determined (sign test) are marked

385   as in (B); pFDR values were calculated as in Fig. 3. Error-related effects in the high-gamma range had a

386   maximum at fronto-central sites at the time of the ERN/Ne peak; at the time of the Pe maximum, the HGB

387   increase was shifted to midline electrodes in a parietal direction.

388   The high-gamma band response, shown here for the time window between 70 and 80

389   Hz, exhibited significantly higher power in error than correct responses. In the time

390   window of the ERN/Ne maximum, the error-related HGB power was centered at fronto-

391   central channels, while it started to shift to more posterior areas around the maximum of

392   the Pe.

393   We calculated Spearman's rank correlation level between the ERN/Ne and Pe amplitude

394   and the error-related spectral modulations in the 70-80 Hz band across subjects. The

395   calculation was done on the signals of the channels with the maximal amplitudes of the

396   components of interest, which was FCz for the ERN/Ne and CPz for the Pe component.

397   There was no significant correlation found. Spearman's rho for the ERN/Ne with error-

398   related HGB components was r_s = -0.05 and p = 0.78, and for Pe r_s = 0.10 and p = 0.58.

399   **Effects of eye movements on high-gamma signals**

400   During the experiments, a great number of miniature eye movements were recorded for

401   each subject. After discarding those events near blinks, on average 6300 ± 2500 (mean

402   ± SD) microsaccades were recorded per subject. To examine the spectral power

403   modulations related to this class of eye movements more closely, we also examined

404   EEG data aligned to the onset of the microsaccades. Fig. 7 shows the group median of

405   those trials. Both at fronto-polar and parieto-central EEG channels, there was a broad-

406   band gamma increase during microsaccade (and saccade, data not shown) onset. This

21

407   increase was prominent from 25 to 120 Hz. In lower frequency bands, e.g., in the delta

408   band, we observed a power decrease, which continued until 500 to 600 ms after the

409   microsaccade onset.

410
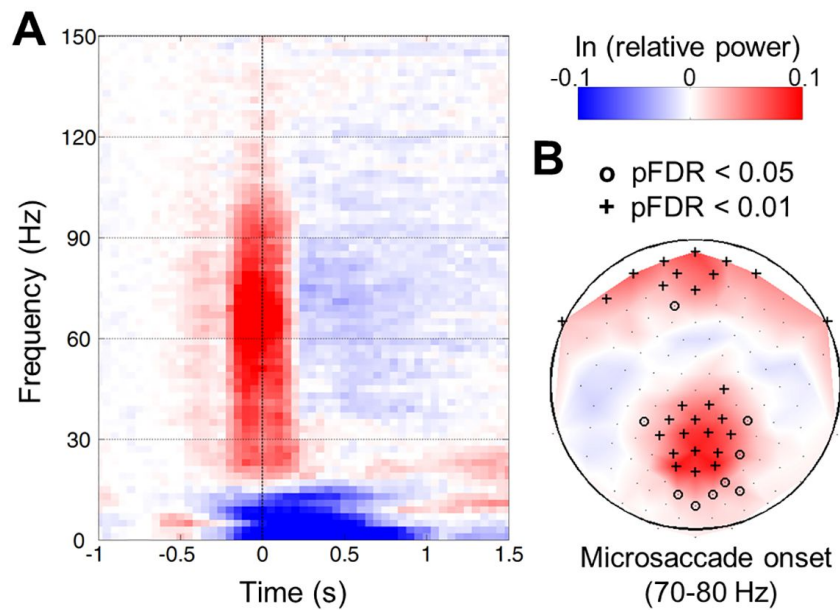
Figure 7: Microsaccade-related time-frequency spectrum in scalp EEG.

412   The plots show a group median of the 31 subjects; the data is aligned to microsaccade onset. **A)** Time-

413   frequency plot of a parieto-central channel (Pz). The log-power (color-coded) was taken relative to a

414   baseline from -1 s to –0.5 s. **B)** Topography of 70-80 Hz high-gamma relative power at the time of

415   microsaccade onset. Electrodes with significant differences are marked with "o" or "+" (sign test,

416   pFDR<0.05 and pFDR<0.01, respectively); pFDR values were calculated as in Fig. 3.

417   Next, in each subject we matched the correct and error condition to have the same

418   amount of microsaccades and saccades within each time-frequency bin of the EEG data

419   after the multitaper analysis. To examine the effect of this measure on the results, we

420   compared the error-related high-gamma activity in matched and unmatched data

421   (Fig. 8).
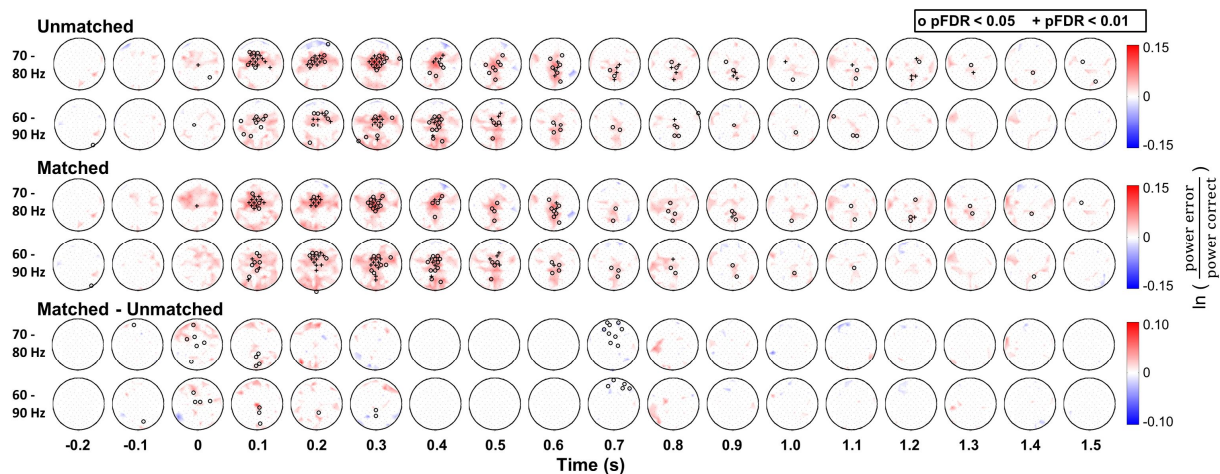
Figure 8: Influence of saccade and microsaccade matching on error-related high-gamma in noninvasive EEG. All plots show group results of the 31 subjects, aligned to EMG response onset. In the top row, error-related high-gamma activity in the 70-80 Hz and 60-90 Hz range is plotted for the data before matching. The middle row depicts the same results after matching each time bin for microsaccade and saccade frequency. In the bottom row, the differences between unmatched and matched data are shown. Significant sites are marked as in Fig. 4.

After the matching, the distribution of electrodes with significant changes in the high-gamma band was only minimally altered, and the overall pattern remained the same. There were only very few significant differences between the original and the matched data. We conclude the error-related effects cannot be attributed to the occurrence of saccades and microsaccades.

Error-related high-gamma activity: frontal vs. parietal regions

We further wished to compare error-related high-gamma activity at frontal and parietal regions as the two major foci of the HGB response. To this aim, we averaged HGB activity in a frontal and a parietal region of interest (ROI).

23
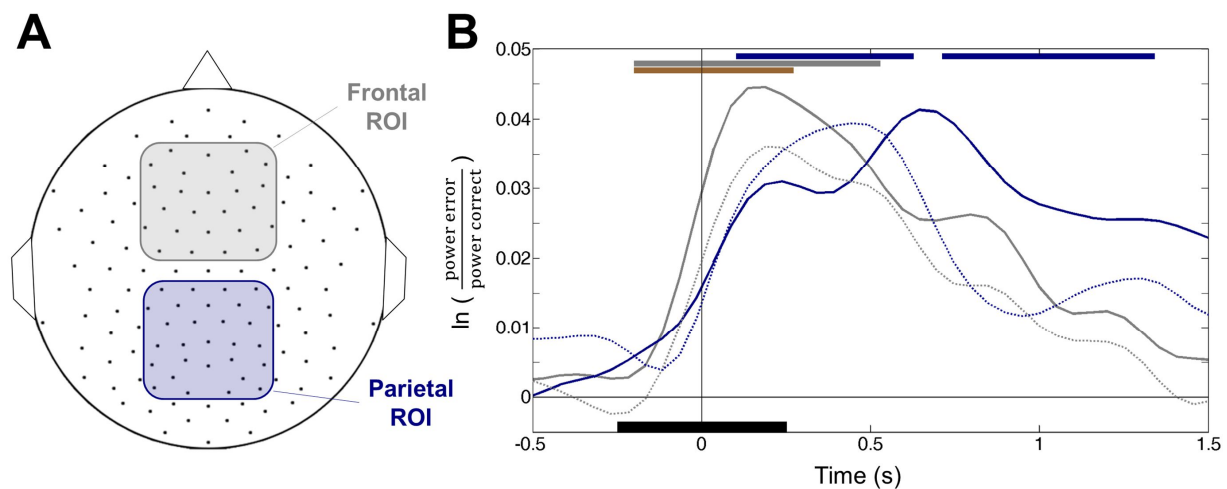
**Figure 9: Time course of error-related 70-80 Hz HGB activity in frontal and parietal regions.**

A) Illustration of the frontal region of interest (ROI) including 25 electrodes (gray) and a parietal ROI with 27 electrodes (blue). **B)** The median error-related 70-80 Hz high-gamma power is plotted for both ROIs in the respective colors; error-related 60-90 Hz power is plotted with dashed lines in the same colors. The bars above indicate times when the 70-80 Hz HGB activity in the frontal (gray), parietal (blue) or difference of both ROIs (brown) was significant (sign test, pFDR<0.01, calculated as in Fig. 6 A). Time point zero represents the response EMG onset. The black bar around 0 s at the bottom of the plot indicates the temporal width of the Gaussian window function (0.5 s) used for the time-resolved spectral density estimation during moving average-calculation, explaining the smoothness of the curves above.

Error-related HGB power in the frontal ROI reached its maximum around 150 to 200 ms after response EMG response onset. The same frequency band in the parietal ROI showed a later peak at 600 to 700 ms. The HGB power in the parietal ROI was significantly increased until up to 1.3 s after the EMG response onset. In the time around the EMG onset, error-related HGB activity in the frontal ROI was significantly (sign test, p<0.01) stronger than in parietal regions.

Confirmation in Intracranial EEG Measurements

Intracranial EEG measurements in 9 patients yielded a multitude of error-related

24

456 changes. For comparability, we concentrated the analysis of error-related high-gamma

457 activity in intracranial EEG to the 60-90 Hz band, as the frequency of interest in

458 noninvasive EEG. An overview of the electrode locations of all 9 patients and sites with

459 significant changes in this range is shown in Fig. 10 together with examples of single-

460 channel time-frequency responses.
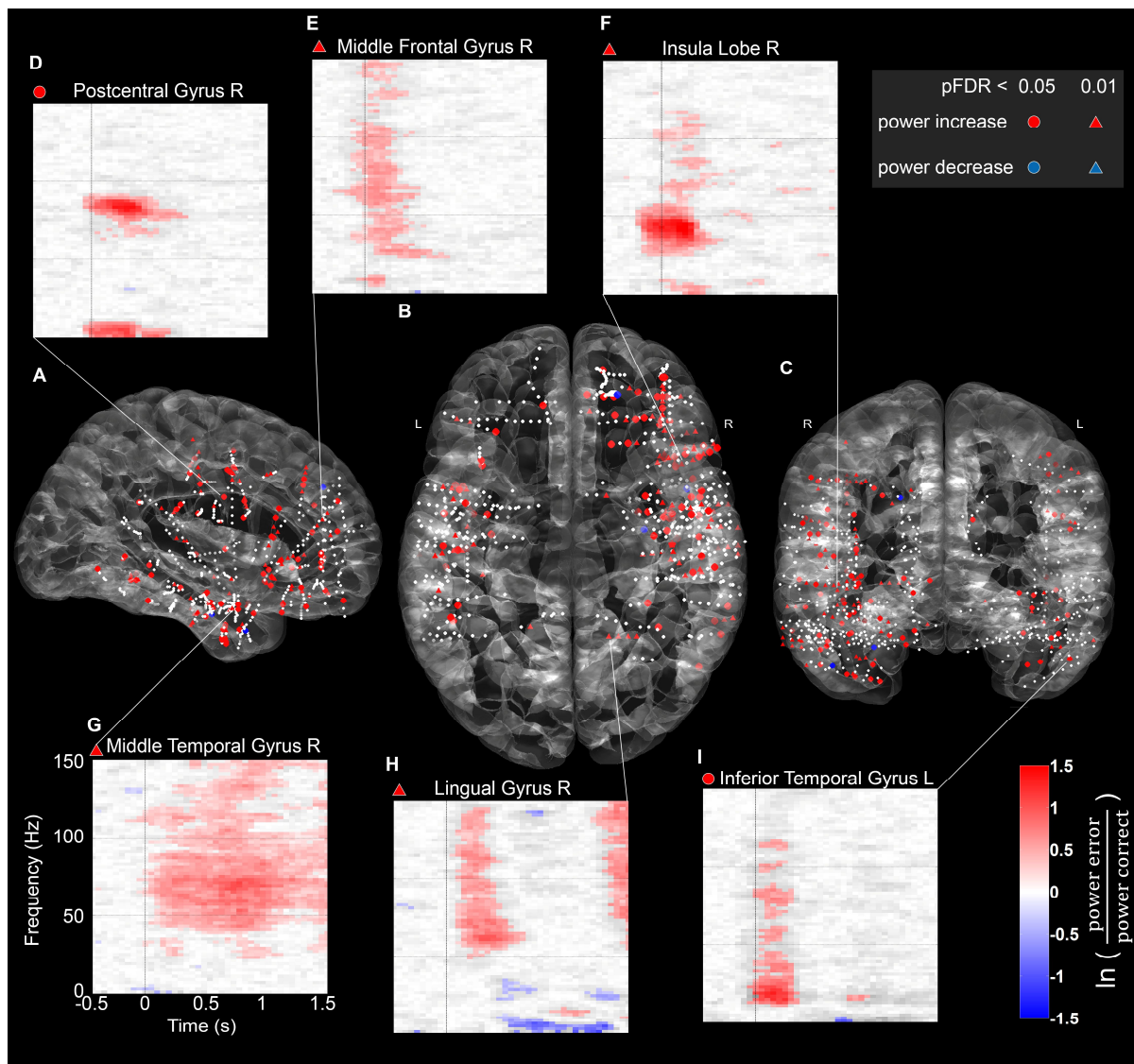
461

462 **Figure 10: Distribution of error-related high-gamma (60-90 Hz) responses in intracranial EEG.**

463 Depth electrodes of 9 epilepsy patients are plotted in white on the semi-transparent ICBM152 brain

464 template from sagittal (A), axial (B), and coronal (C) views. Sites with significant activations in the 60-90

465 Hz range in the time of interest between 0 s and 0.6 s after an error, as identified in noninvasive EEG,

25

466 were marked with colored circles or triangles (sign test, pFDR<0.05 or pFDR<0.01, calculation of pFDR

467 values across all channels). The marker color indicates whether there was a relative power increase (red)

468 or decrease (blue) compared to correct responses. Exemplary single-channel time-frequency plots are

469 shown above and below together with their assignment to anatomical areas; time-frequency bins with

470 pFDR>0.05 are shown grayed out (calculation of pFDR across 51 times (-0.75 s to 1.75 s, 50 ms steps)

471 and 126 frequencies (0-250 Hz, 2 Hz steps). Color scale as in Fig. 6 C.

472 Error-related high-gamma modulations were found in multiple areas across the cortex,

473 mostly manifesting as power increases relative to correct responses. As is noticeable in

474 the exemplary time-frequency plots, we observed different types of error-related HGB

475 modulations in intracranial EEG. Firstly, responses with a clear maximum which was

476 restricted to a small area in time and frequency, as the examples from the postcentral

477 gyrus and the insula (Fig. 10 D,F). Secondly, responses with a transient, broadband

478 gamma increase, e.g., in the middle frontal gyrus, the lingual gyrus or the inferior

479 temporal gyrus (Fig. 10 E,H,I). Thirdly, responses with a broad-band gamma increase

480 and with a long duration of around 2 s, e.g., in the middle temporal gyrus (Fig. 10 G).

481 More significant HGB modulations were located in the right hemisphere; however, it is to

482 note that our sample consisted of more electrodes in the right hemisphere (443 sites

483 after bipolar re-referencing & channel rejection) compared to the left hemisphere (247

484 sites). Across the 9 patients, we observed an average error rate of 21.09 ± 0.11 (mean ±

485 SD) % with the left hand, and 20.81 ± 0.10 % with the right hand; there was no

486 significant difference with p=0.46 (paired one-sided t-test).

487 To get an overview of the significance of single-channel observations, we calculated the

488 ratio of significant responses within 19 regions of interest (Table 1).

26

489 **Table 1: Significant error-related 60-90 Hz power modulations in different areas.**

490 For 19 ROIs, the percentages of channels with significant (pFDR<0.05) 60-90 Hz HGB error-related power

491 modulations, averaged across the time window from 0 s to 0.6 s after the response (FDR-corrected over

492 all channels, as in Fig. 10), are listed together with the total number of channels (n) included per area.

Area	n	% positive	% negative
Heschls gyrus	2	100.00	0.00
Lingual gyrus	8	62.50	0.00
Middle frontal gyrus	35	45.71	0.00
Precentral gyrus	43	44.19	0.00
Insular cortex	47	38.30	0.00
Inferior frontal gyrus	71	33.80	0.00
Postcentral gyrus	40	30.00	0.00
Fusiform gyrus	39	28.21	0.00
Middle cingulate cortex	4	25.00	0.00
Supramarginal gyrus	25	24.00	0.00
Inferior temporal gyrus	72	23.61	0.00
Hippocampal area	60	18.33	1.67
Orbitofrontal cortex	73	17.81	0.00
Superior temporal gyrus	35	17.14	0.00
Superior frontal gyrus	22	13.64	4.55
Middle temporal gyrus	117	12.82	0.85
Anterior cingulate cortex	24	8.33	0.00
Rolandic operculum	25	4.00	0.00
Precuneus	6	0.00	0.00

493

494 Error-related high-gamma power increases were observed in 18 of the 19 ROIs, with a

495 range of 4 % to 100 % of involved electrodes in the different areas. Power decreases

496 were only observed in 3 regions, ranging from 0.85 % to 4.55 % of electrodes.

497 We further compared error-related spectral power modulations of nearby intracranial

498 EEG and scalp EEG electrodes in the range of the motor cortex (Fig. 11).

27
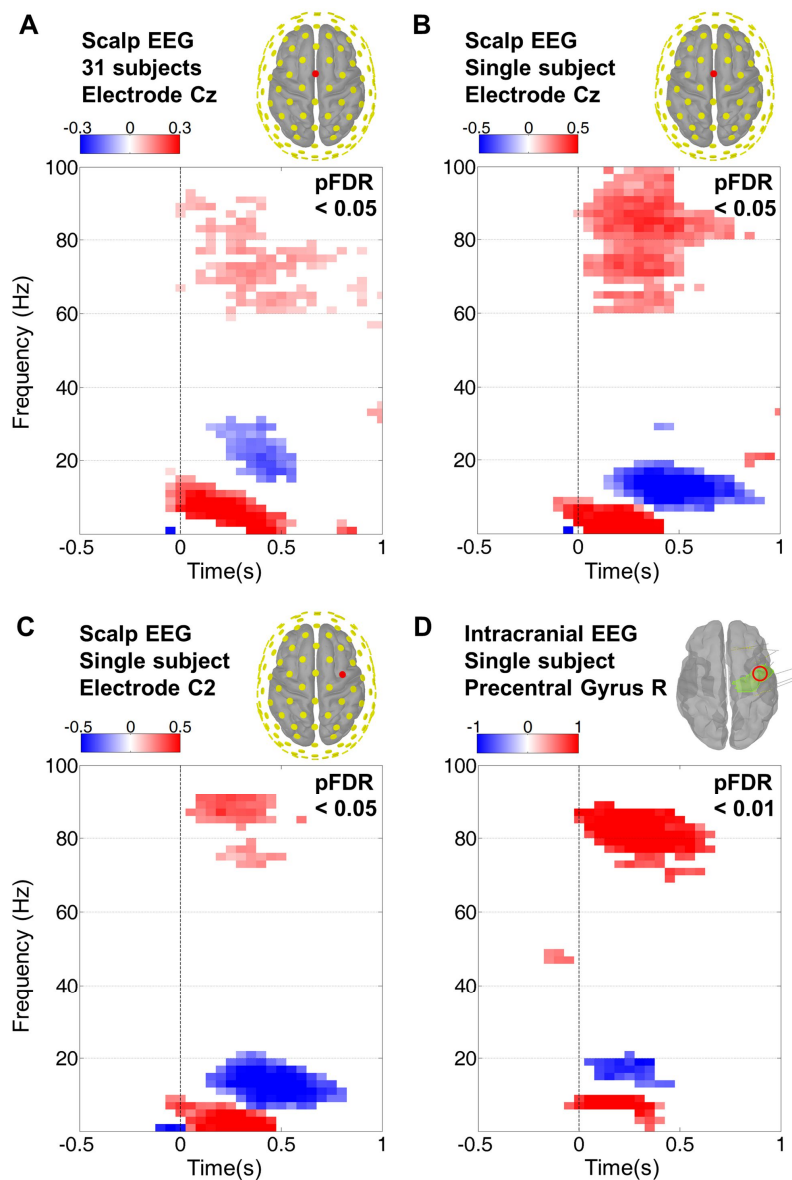
Figure 11: Comparison of intracranial EEG with scalp EEG in group and single subject results.

The color scale depicts the logarithmic relative power of the median error-related response baselined with the correct response. Only significant power modulations are shown with the threshold as labeled in the top right corner of the respective plot. Calculation of pFDR-values was done with an FDR-corrected Wilcoxon rank sum test (single subjects) and an FDR-corrected sign test (group results). **A)** Group median (31 subjects) of error-related spectral power modulations at electrode Cz. **B)** Single-subject error-related spectral power modulations in EEG at electrode Cz. **C)** Single-subject error-related spectral power modulations in EEG at electrode C2. **D)** Single-subject error-related spectral power modulations in intracranial EEG within the right precentral gyrus in close proximity of the C2 electrode standard position.

509   Both in scalp EEG at central positions and intracranial EEG in the precentral gyrus,

510   significant error-related power modulations were observed in the delta, theta, alpha,

511   beta, and high-gamma band. In these examples, the spectral patterns of nearby

512   intracranial and noninvasive EEG channels were very similar at both group and single-

513   subject level (Fig. 11). In intracranial EEG, the high-gamma activity had the strongest

514   error-related power modulation, while in noninvasive measurements, the lower

515   frequency bands showed a greater difference between correct and error responses.

516   **Fine-grained dynamics of error-related activity in intracranial EEG**

517   For a closer look at the spatio-temporal progression of error-related activity across the

518   brain, we analyzed the time course of error-related low- and high-spectral power

519   modulations in the intracranially recorded data of all 9 patients (Fig. 12).
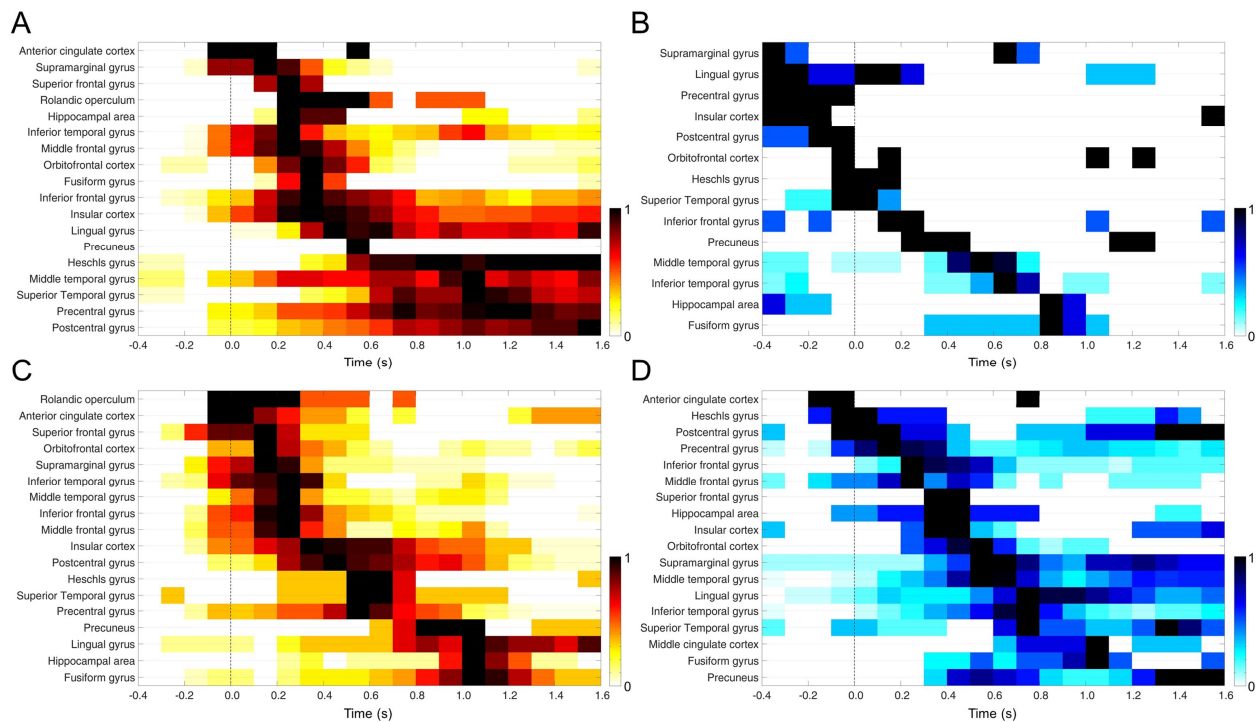
Figure 12: Time course of significant error-related power modulations in intracranial EEG.
For each area, the total number of significant increases (red) and decreases (blue) in all patients were normalized; the areas were sorted according to the time with the maximal count (equal to 1) in ascending order. Time course of HGB power modulations in the range 50-120 Hz are shown at the top (A, B), low-frequency components below 30 Hz are shown at the bottom (C, D). The data is aligned to response onset.

It is apparent that low and high frequencies, as well as power increases and decreases, differed in their spatial distribution over time. Subareas in frontal, temporal, and parietal brain regions were activated at various time points before, during and after the error response. Error-related increases in the high-gamma range (Fig. 12 A) especially exhibited a temporal development that started at frontal surface und deep areas, including the ACC, and then advanced to both parietal and temporal regions of the brain. Notably, increased error-related HGB activity in hippocampal areas peaked 0.3 s after the response, while decreased hippocampal HGB activity (Fig. 12 B) occurred -0.4

535   to -0.2 s before the response and again 0.8 to 1.0 s after the response. Overall,

536   intracranial EEG portrays a consistent but much more complex picture of error

537   processing compared to noninvasive data.

Discussion

539   Converging evidence indicates an important role of HGB activity in cortical function

540   (Başar et al., 2001; Herrmann et al., 2004a; Fries, 2005; Canolty et al., 2006; Crone et

541   al., 2006; Jensen et al., 2007; Jerbi et al., 2009b; Buzsáki and Wang, 2012). Studies on

542   human HGB activity were initially restricted to intracranial EEG (Szurhaj and Derambure,

543   2006; Miller et al., 2007; Whitham et al., 2008). A growing body of literature, however,

544   indicates that HGB activity can be measured noninvasively using EEG

545   (Muthukumaraswamy, 2013). HGB activity has been measured noninvasively during

546   sensory stimulation (Cobb and Dawson, 1960; Heinrich and Bach, 2004; Scheller et al.,

547   2005), cognitive processing (Friese et al., 2013; Long et al., 2014), executed (Ball et al.,

548   2008; Darvas et al., 2010; Nottage et al., 2013) and imagined motor tasks (Smith et al.,

549   2014). This wealth of noninvasive HGB demonstrations underscores that it is in principle

550   possible to measure HGB activity noninvasively. While error-related HGB activity has

551   been demonstrated in intracranial EEG (Milekovic et al., 2013; Bastin et al., 2017), here

552   we show error-related HGB activity noninvasively.

553   In the present study, we examined error processing in the human brain as reflected in

554   HGB activity, based on measurements using noninvasive and intracranial EEG. In both,

555   we found significant error-related modulations of high-gamma power. Noninvasive 128-

556   channel EEG in an electromagnetically shielded cabin enabled us to reveal the global

557 topography and dynamics of event-related potentials and spectral power modulations,

558 while we used intracranial EEG to validate the noninvasive findings, and additionally to

559 probe local fine-grained activity patterns.

560 **Error-related low-frequency responses in noninvasive EEG**

561 Our findings generally reproduced the spectral power modulations in the delta, theta,

562 alpha and beta bands in noninvasive EEG as reported by previous studies (Luu et al.,

563 2004; Yordanova et al., 2004; Kolev et al., 2005; Trujillo and Allen, 2007; Koelewijn et

564 al., 2008; Carp and Compton, 2009). Further, our results also revealed several

565 unreported topographical features.

566 For example, we observed an error-related delta band pattern characterized by the co-

567 occurrence of increased and decreased power in anterior and posterior regions,

568 respectively (Fig. 4,6). In the high-beta and low-gamma band (20 - 40 Hz), we observed

569 an error-related power increase in a late time window, starting 800 ms after the

570 response (Fig. 4,6). Interestingly, around 1000 ms after response onset, a second (with

571 the ERN/Ne being the first) smaller but significant (p<0.01) negative deflection in the

572 error-related potential occurred at midline EEG channels (Fig. 4, bottom row) which thus

573 might be termed "Ne1000". The maximal low-gamma band response occurred at roughly

574 the same time with a focus on midline channels. Together, these examples illustrate that

575 an optimized EEG procedure applied to a suitably large group of subjects can reveal a

576 range of additional significant features of the error-related response that may be useful

577 to consider in future studies.

578

Error-related high-frequency responses in noninvasive EEG

579

580 Both in group results and single subjects, we found significant error-related HGB power

581 increases. Although high-gamma activity was seen in both correct and erroneous trials,

582 it was significantly stronger in the erroneous trials. The error-related high-gamma

583 response presented itself as an early fronto-central power increase, followed by a shift to

584 parieto-central areas, where the HGB power after errors was significantly larger than

585 than after correct responses over an extended period (up to 1.5 s, see Fig. 4,9).

586 Importantly, the spatio-temporal dynamics differed clearly from those of theta, alpha,

587 beta, and low-gamma responses, and high-gamma response were not correlated to

588 ERN/Ne and Pe amplitudes across subjects, pointing to a unique functional role.

589 We controlled thoroughly for ocular artifacts in our noninvasive EEG experiments.

590 Firstly, by using high-resolution binocular eye tracking, we were able to exactly match

591 each time bin of the error-related and non-error-related time-frequency-resolved data for

592 both microsaccade and saccade frequency and thus avoid a differential effect of ocular

593 potentials (Yuval-Greenberg et al., 2008) on the error-related high-gamma signals.

594 Secondly, the topography of microsaccade-related HGB effects showed a qualitatively

595 different spatial pattern compared to the error-related HGB responses (Fig. 7, 8). Thus,

596 we conclude that our error-related HGB responses cannot be explained as ocular

597 artifacts.

598 Further, we also think that it is highly unlikely that our error-related HGB responses

599 reflect EMG contamination. First, the error-related HGB power did not exhibit the rather

600 flat, broadband power increase typical of EMG contamination (Goncharova et al., 2003),

601 but rather a strong maximum between 60 and 90 Hz. Second, the spatial distribution of

33

602 the high-gamma increase with the maximum over the midline differed from that to be

603 expected for EMG, which has its emphasis on peripheral electrodes close to the

604 muscles (Goncharova et al., 2003; Whitham et al., 2007).

605 **Error-related high-gamma responses in intracranial EEG**

606 Error-related intracranial high-gamma activity was found at multiple locations in the

607 brain, showing much larger amplitudes than the extracranial counterparts. These areas

608 overlapped strongly with areas where intracranial error-related potentials and HGB

609 increases were previously reported (Brázdil et al., 2005; Bastin et al., 2017). In addition

610 to gamma increases, we also observed responses with a decreased relative high-

611 gamma power in relation to errors. They often followed a HGB power increase, possibly

612 representing a systematic suppression aftereffect. As saccadic artifacts in intracranial

613 EEG are mainly limited to the temporal pole (Jerbi et al., 2009a), our intracranially

614 recorded error-related HGB increases together with the results reported in 6 patients by

615 Bastin et al. (2017) clearly show the existence of such responses on the cortex.

616 Furthermore, as illustrated by Fig. 12, intracranial and scalp EEG channels placed

617 above central brain regions showed coinciding time-frequency patterns in their error-

618 related responses (see Fig. 12). Together, these observations lend additional support to

619 the validity of our noninvasive data. One limitation of such a comparison is, of course,

620 that not all areas can be observed in noninvasive EEG recordings. While we assume

621 signals from the hippocampus and insular cortex to be virtually undetectable in

622 noninvasive EEG, signals from cingular areas might be recordable from the surface (Ball

623 et al., 1999). Generally, the superficial regions of the cortex areas can be expected to

624 have a greater influence on the scalp EEG than subcortical areas (Nunez et al., 1997).

34

625   The time course of intracranial activations (Fig. 13) confirmed that frontal regions were

626   activated rather early, while parietal (as well as temporal) areas became active later, in

627   line with a downstream role in error processing. Intracranial data also clearly showed

628   that, expectedly, cortical error processing is more complex than what can be observed in

629   noninvasive EEG. Hippocampal high-gamma was significantly decreased prior to the

630   actual error, and increased after the error. This could signify an interaction of error and

631   memory systems, consistent with a role of gamma in memory functions (Howard et al.,

632   2003; Jensen et al., 2007; Sederberg et al., 2007; Kucewicz et al., 2014, 2017).

633   Furthermore, Fig. 13 also demonstrates that lower HGB power in pre-, postcentral, and

634   supramarginal gyri as well as the insular cortex may precede errors. One explanation for

635   that could be that high-gamma power could indicate a pre-activation or "readiness" of a

636   brain area.

Interpretation of high-gamma band activity

638   Broadband power modulations in intracranial EEG are positively correlated with the local

639   single-neuron firing rate in humans (Manning et al., 2009) and can be explained by

640   current models (Bédard et al., 2006; Ray et al., 2008; Miller et al., 2009), which assume

641   a linear low-pass kernel to quantify the influence of single synaptic events on the

642   population signal. Insofar as the underlying spiking activity can be assumed to

643   sufficiently irregular (Softky and Koch, 1993; London et al., 2010), the presynaptic action

644   potentials can be modeled as a Poisson process, which has a broad spectrum

645   contributing equally at all frequencies. Some characteristics of the average kernel

646   proposed in these previous works, such as the cutoff frequency and the order of the low-

647   pass filtering, have been experimentally investigated (Miller et al., 2009). Our present

35

648   EEG results are consistent with broadband changes across a wide frequency range (Fig.

649   2-5), possibly reflecting similar mechanisms as previously described in intracranial data.

650   In addition to broadband changes, inhibitory coupling may lead to gamma oscillations

651   manifesting in more narrow-banded peaks in different ways. If fluctations of the

652   membrane potential are small, e.g., if the neurons are driven tonically, inhibitory

653   connections can serve to synchronize the activity in the population, leading to regular

654   and globally synchronous firing (Wang and Buzsáki, 1996; White et al., 1998; Kopell et

655   al., 2000).

656   In contrast, the mechanism of a collective oscillatory instability relies on inhibitory

657   feedback arriving with a temporal delay d; oscillatory frequencies are in the range of $\frac{1}{2d}$

658   and $\frac{1}{4d}$ (Brunel and Hakim, 1999; Tiesinga and José, 2000), thus well typically in the

659   high gamma range. The oscillation in these states persists on the population level - it is

660   manifest in the pairwise correlations between neurons - while single cells exhibit

661   irregular firing (Brunel and Hakim, 1999; Brunel, 2000; Tiesinga and José, 2000; Brunel

662   and Wang, 2003).

663   Another network mechanism that can give rise to gamma oscillations relies on the

664   feedback loop between excitatory (E) and inhibitory (I) neurons (Wilson and Cowan,

665   1972), requiring a strong coupling from E to I and from I to E (reviewed in Buzsáki and

666   Wang, 2012). The resulting oscillations in spiking network models are typically in the

667   lower gamma range (Brunel and Wang, 2003). This mechanism has also been

668   employed in a non-linear rate model to explain the dependence of gamma oscillation

669   frequency on the stimulus size in visual cortex, exploiting the modulation of the intra-

36

670 cortical E-I feedback loop through the neuronal non-linearity (Kang et al., 2010). Notably,

671 the gamma frequency peak around 80 Hz observed in our data shows a similarity to the

672 gamma frequency profiles predicted by the model by Brunel (2000, Fig. 9 A).

673 Also, more realistic networks comprised of several layers (Potjans and Diesmann, 2014)

674 are able to generate an oscillation in the same frequency range: A mean-field analysis

675 shows that the network mechanism is here a subcircuit comprised of excitatory and

676 inhibitory neurons in layers 2/3 and 4 (Bos et al., 2016). The mathematical analysis of

677 these networks also exposes why the power of the oscillation is strongly influenced by

678 the tonic drive to the network, predominantly to layer 4. An error-related signal changing

679 the tonic drive to the local oscillation-generating network may thus be a candidate

680 mechanism behind the observed modulations in the power spectra. Such a mechanism

681 would predict a co-modulation of the multi-unit firing rate with the increase of gamma

682 power, as previously empirically observed (Nir et al. 2007) and very much in line with our

683 observation of a co-occurrence of both, broad band changes and additionally enhanced

684 gamma power around 80 Hz (Fig 2-5). Thus, a distinction between a broadband

685 increase of gamma power by the firing rate alone from a modulation of intrinsic

686 oscillatory properties of the circuit may thus not be as clear cut.

687 From our present results we still cannot draw firm conclusions about the mechanisms

688 giving rise to the enhanced gamma activity that we have prominently observed around

689 80 Hz and beyond. To gain such insight in future studies, our noninvasive EEG method

690 may prove to be a useful tool to study gamma responses and they mechanistic

691 underpinnings.

692

37

693 **Functional relevance of error-related HGB activity**

694 Our findings reveal sustained, significant HGB activity over the parietal cortex that

695 substantially outlasted the duration of the Pe, up to at least 1.5 s after response onset.

696 This raises the question whether this specific timing may hint at a possible functional

697 role of this late high-gamma response during error processing. Generally, processing of

698 behavioral errors involves several prominent functional sub-processes. These range

699 from precursors of error detection, such as the evaluation of actual and intended action

700 outcomes, including perceptual evidence accumulation, over the explicit error detection

701 itself, to the evaluation of error importance, error-related learning, and behavioral

702 adjustment (Holroyd and Coles, 2002; Carbonnell and Falkenstein, 2006; Taylor et al.,

703 2007). Much research so far has focused on how these processes relate to the ERN/Ne

704 and Pe complex. Recent evidence, based on systematic reward manipulations that

705 targeted the criterion which participants used to decide whether or not to report errors,

706 has linked the Pe to the strength of accumulated error-related evidence (Steinhauser

707 and Yeung, 2010). Late, sustained parietal high-gamma activity could thus reflect

708 processes downstream to error evidence accumulations, such as behavioral adjustment

709 and motor learning. This speculation could be tested in future studies utilizing EEG-

710 based HGB mapping as described in our present study.

711 **Conclusion & Outlook**

712 The fact that error-related HGB signals are detectable with noninvasive EEG opens up a

713 much wider avenue of research than would be feasible with intracranial recordings

714 alone, particularly in healthy subjects and also in populations of patients with different

715 neuropsychiatric disorders, such as social phobias, autism spectrum disorders,

38

716 schizophrenia, depression, as well as obsessive-compulsive disorder – all of which have

717 been connected with alterations in the neural response to behavioral errors (Alain et al.,

718 2002; Hajcak and Simons, 2002; Hajcak et al., 2003; Henderson et al., 2006; Ruchsow

719 et al., 2006; Shiels and Hawk, 2010; Riesel et al., 2011). Implantation of intracranial

720 electrodes is confined to a much smaller group of patients undergoing pre-neurosurgical

721 evaluation, in most cases for the treatment of focal pharmacoresistant epilepsy. Our

722 findings however clearly highlight the unique value of these intracranial recordings. For

723 example, they allow assessment of brain structures that are difficult or even impossible

724 to probe electrophysiological noninvasively, such as insular cortex and the hippocampal

725 formation.

726 Our findings could help understanding the mechanisms behind human error processing.

727 Further, they could also help in the decoding of errors from single-trial EEG using

728 machine learning algorithms to improve the performance of brain-machine interfacing

729 (Ferrez and Millan, 2008; Kreilinger et al., 2012; Spüler et al., 2012; Milekovic et al.,

730 2013; Völker et al., 2017). To dissect underlying mechanisms, an examination of phase-

731 amplitude coupling between high-gamma power and lower frequency bands (Canolty et

732 al., 2006; Cohen et al., 2008; Tort et al., 2010; Friese et al., 2013) during error

733 processing could provide valuable information. More generally, we suggest that parallel

734 investigations of error processing with both noninvasive as well as invasive recordings,

735 and with attention to both classical error-related potentials as well as high-frequency

736 signatures of error processing, might prove as the most fruitful way towards

737 understanding the neural basis of this fundamental facet of cognition.

39

References

738

739 Alain C, McNeely HE, He Y, Christensen BK, West R (2002) Neurophysiological Evidence of
740   Error-monitoring Deficits in Patients with Schizophrenia. Cereb Cortex 12:840–846.

741 Albrecht B, Heinrich H, Brandeis D, Uebel H, Yordanova J, Kolev V, Rothenberger A,
742   Banaschewski T (2009) Flanker-Task in Children. J Psychophysiol 23:183–190.

743 Amunts K, Schleicher A, Zilles K (2007) Cytoarchitecture of the cerebral cortex—More than
744   localization. NeuroImage 37:1061–1065.

745 Ball T, Demandt E, Mutschler I, Neitzel E, Mehring C, Vogt K, Aertsen A, Schulze-Bonhage A
746   (2008) Movement related activity in the high gamma range of the human EEG.
747   NeuroImage 41:302–310.

748 Ball T, Schreiber A, Feige B, Wagner M, Lücking CH, Kristeva-Feige R (1999) The Role of
749   Higher-Order Motor Areas in Voluntary Movement as Revealed by High-Resolution EEG
750   and fMRI. NeuroImage 10:682–694.

751 Başar E, Başar-Eroglu C, Karakaş S, Schürmann M (2001) Gamma, alpha, delta, and theta
752   oscillations govern cognitive processes. Int J Psychophysiol 39:241–248.

753 Bastin J, Deman P, David O, Gueguen M, Benis D, Minotti L, Hoffman D, Combrisson E, Kujala
754   J, Perrone-Bertolotti M, Kahane P, Lachaux J-P, Jerbi K (2017) Direct Recordings from
755   Human Anterior Insula Reveal its Leading Role within the Error-Monitoring Network.
756   Cereb Cortex 27:1545–1557.

757 Bédard C, Kröger H, Destexhe A (2006) Does the 1/f frequency scaling of brain signals reflect
758   self-organized critical states? Phys Rev Lett 97:118102.

759 Benjamini Y, Hochberg Y (1995) Controlling the False Discovery Rate: A Practical and
760   Powerful Approach to Multiple Testing. J R Stat Soc Ser B Methodol 57:289–300.

761 Bos H, Diesmann M, Helias M (2016) Identifying Anatomical Origins of Coexisting Oscillations
762   in the Cortical Microcircuit. PLoS Comput Biol 12:e1005132.

763 Botvinick M, Nystrom LE, Fissell K, Carter CS, Cohen JD (1999) Conflict monitoring versus
764   selection-for-action in anterior cingulate cortex. Nature 402:179–181.

765 Brainard DH (1997) The psychophysics toolbox. Spat Vis 10:433–436.

766 Brázdil M, Roman R, Daniel P, Rektor I (2005) Intracerebral Error-Related Negativity in a
767   Simple Go/NoGo Task. J Psychophysiol 19:244–255.

768 Brunel N (2000) Dynamics of sparsely connected networks of excitatory and inhibitory spiking
769   neurons. J Comput Neurosci 8:183–208.

770   Brunel N, Hakim V (1999) Fast global oscillations in networks of integrate-and-fire neurons with
771   low firing rates. Neural Comput 11:1621–1671.

772   Brunel N, Wang X-J (2003) What Determines the Frequency of Fast Network Oscillations With
773   Irregular Neural Discharges? I. Synaptic Dynamics and Excitation-Inhibition Balance. J
774   Neurophysiol 90:415–430.

775   Buzsáki G, Wang X-J (2012) Mechanisms of Gamma Oscillations. Annu Rev Neurosci 35:203–
776   225.

777   Canolty RT, Edwards E, Dalal SS, Soltani M, Nagarajan SS, Kirsch HE, Berger MS, Barbaro
778   NM, Knight RT (2006) High Gamma Power Is Phase-Locked to Theta Oscillations in
779   Human Neocortex. Science 313:1626–1628.

780   Carbonnell L, Falkenstein M (2006) Does the error negativity reflect the degree of response
781   conflict? Brain Res 1095:124–130.

782   Carp J, Compton RJ (2009) Alpha power is influenced by performance errors. Psychophysiology
783   46:336–343.

784   Cobb WA, Dawson GD (1960) The latency and form in man of the occipital potentials evoked by
785   bright flashes. J Physiol 152:108–121.

786   Cohen MX, Elger CE, Fell J (2008) Oscillatory Activity and Phase–Amplitude Coupling in the
787   Human Medial Frontal Cortex during Decision Making. J Cogn Neurosci 21:390–402.

788   Crone NE, Miglioretti DL, Gordon B, Lesser RP (1998) Functional mapping of human
789   sensorimotor cortex with electrocorticographic spectral analysis. II. Event-related
790   synchronization in the gamma band. Brain J Neurol 121 (Pt 12):2301–2315.

791   Crone NE, Sinai A, Korzeniewska A (2006) High-frequency gamma oscillations and human
792   brain mapping with electrocorticography. In: Progress in Brain Research (Klimesch CN
793   and W, ed), pp 275–295 Event-Related Dynamics of Brain Oscillations. Elsevier.

794   Darvas F, Scherer R, Ojemann JG, Rao RP, Miller KJ, Sorensen LB (2010) High gamma
795   mapping using EEG. NeuroImage 49:930–938.

796   Dixon WJ, Mood AM (1946) The Statistical Sign Test. J Am Stat Assoc 41:557–566.

797   Eickhoff SB, Heim S, Zilles K, Amunts K (2006) Testing anatomically specified hypotheses in
798   functional imaging using cytoarchitectonic maps. NeuroImage 32:570–582.

799   Eickhoff SB, Paus T, Caspers S, Grosbras M-H, Evans AC, Zilles K, Amunts K (2007)
800   Assignment of functional activations to probabilistic cytoarchitectonic areas revisited.
801   NeuroImage 36:511–521.

802   Eickhoff SB, Stephan KE, Mohlberg H, Grefkes C, Fink GR, Amunts K, Zilles K (2005) A new
803   SPM toolbox for combining probabilistic cytoarchitectonic maps and functional imaging
804   data. NeuroImage 25:1325–1335.

41

805 Engbert R, Kliegl R (2003) Microsaccades uncover the orientation of covert attention. Vision Res
806   43:1035–1045.

807 Eriksen CW, Eriksen BA (1979) Target redundancy in visual search: Do repetitions of the target
808   within thedisplay impair processing? Percept Psychophys 26:195–205.

809 Falkenstein M, Hohnsbein J, Hoormann J, Blanke L (1991) Effects of crossmodal divided
810   attention on late ERP components. II. Error processing in choice reaction tasks.
811   Electroencephalogr Clin Neurophysiol 78:447–455.

812 Ferrez PW, Millan J del R (2008) Error-Related EEG Potentials Generated During Simulated
813   Brain #x2013;Computer Interaction. IEEE Trans Biomed Eng 55:923–929.

814 Fonov V, Evans A, McKinstry R, Almli C, Collins D (2009) Unbiased nonlinear average age-
815   appropriate brain templates from birth to adulthood. NeuroImage 47, Supplement 1:S102.

816 Freeman WJ, Rogers LJ, Holmes MD, Silbergeld DL (2000) Spatial spectral analysis of human
817   electrocorticograms including the alpha and gamma bands. J Neurosci Methods 95:111–
818   121.

819 Fries P (2005) A mechanism for cognitive dynamics: neuronal communication through neuronal
820   coherence. Trends Cogn Sci 9:474–480.

821 Friese U, Köster M, Hassler U, Martens U, Trujillo-Barreto N, Gruber T (2013) Successful
822   memory encoding is associated with increased cross-frequency coupling between frontal
823   theta and posterior gamma oscillations in human scalp-recorded EEG. NeuroImage
824   66:642–647.

825 Gehring WJ, Goss B, Coles MGH, Meyer DE, Donchin E (1993) A Neural System for Error
826   Detection and Compensation. Psychol Sci 4:385–390.

827 Gehring WJ, Knight RT (2000) Prefrontal–cingulate interactions in action monitoring. Nat
828   Neurosci 3:516–520.

829 Goncharova II, McFarland DJ, Vaughan TM, Wolpaw JR (2003) EMG contamination of EEG:
830   spectral and topographical characteristics. Clin Neurophysiol 114:1580–1593.

831 Hajcak G, McDonald N, Simons RF (2003) Anxiety and error-related brain activity. Biol Psychol
832   64:77–90.

833 Hajcak G, Simons RF (2002) Error-related brain activity in obsessive–compulsive
834   undergraduates. Psychiatry Res 110:63–72.

835 Heinrich SP, Bach M (2004) High-frequency oscillations in human visual cortex do not mirror
836   retinal frequencies. Neurosci Lett 369:55–58.

837 Henderson H, Schwartz C, Mundy P, Burnette C, Sutton S, Zahka N, Pradella A (2006) Response
838   monitoring, the error-related negativity, and differences in social behavior in autism.
839   Brain Cogn 61:96–109.

840 Herrmann CS, Munk MHJ, Engel AK (2004a) Cognitive functions of gamma-band activity:
841   memory match and utilization. Trends Cogn Sci 8:347–355.

842 Herrmann MJ, Römmler J, Ehlis A-C, Heidrich A, Fallgatter AJ (2004b) Source localization
843   (LORETA) of the error-related-negativity (ERN/Ne) and positivity (Pe). Cogn Brain Res
844   20:294–299.

845 Holroyd CB, Coles MGH (2002) The neural basis of human error processing: reinforcement
846   learning, dopamine, and the error-related negativity. Psychol Rev 109:679–709.

847 Howard MW, Rizzuto DS, Caplan JB, Madsen JR, Lisman J, Aschenbrenner-Scheibe R, Schulze-
848   Bonhage A, Kahana MJ (2003) Gamma Oscillations Correlate with Working Memory
849   Load in Humans. Cereb Cortex 13:1369–1374.

850 Jensen O, Kaiser J, Lachaux J-P (2007) Human gamma-frequency oscillations associated with
851   attention and memory. Trends Neurosci 30:317–324.

852 Jerbi K, Freyermuth S, Dalal S, Kahane P, Bertrand O, Berthoz A, Lachaux J-P (2009a) Saccade
853   Related Gamma-Band Activity in Intracerebral EEG: Dissociating Neural from Ocular
854   Muscle Activity. Brain Topogr 22:18–23.

855 Jerbi K, Ossandón T, Hamamé CM, Senova S, Dalal SS, Jung J, Minotti L, Bertrand O, Berthoz
856   A, Kahane P, Lachaux J-P (2009b) Task-related gamma-band dynamics from an
857   intracerebral perspective: Review and implications for surface EEG and MEG. Hum
858   Brain Mapp 30:1758–1771.

859 Kang K, Shelley M, Henrie JA, Shapley R (2010) LFP spectral peaks in V1 cortex: network
860   resonance and cortico-cortical feedback. J Comput Neurosci 29:495–507.

861 Koelewijn T, van Schie HT, Bekkering H, Oostenveld R, Jensen O (2008) Motor-cortical beta
862   oscillations are modulated by correctness of observed action. NeuroImage 40:767–775.

863 Kolev V, Falkenstein M, Yordanova J (2005) Aging and error processing - Time-frequency
864   analysis of error-related potentials. J Psychophysiol 19:289–297.

865 Kopell N, Ermentrout GB, Whittington MA, Traub RD (2000) Gamma rhythms and beta rhythms
866   have different synchronization properties. Proc Natl Acad Sci U S A 97:1867–1872.

867 Kopp B, Rist F, Mattler U (1996) N200 in the flanker task as a neurobehavioral tool for
868   investigating executive control. Psychophysiology 33:282–294.

869 Kreilinger A, Neuper C, Müller-Putz GR (2012) Error potential detection during continuous
870   movement of an artificial arm controlled by brain–computer interface. Med Biol Eng
871   Comput 50:223–230.

872 Kucewicz MT, Berry BM, Kremen V, Brinkmann BH, Sperling MR, Jobst BC, Gross RE, Lega
873   B, Sheth SA, Stein JM, Das SR, Gorniak R, Stead SM, Rizzuto DS, Kahana MJ, Worrell
874   GA (2017) Dissecting gamma frequency activity during human memory processing. Brain
875   140:1337–1350.

876   Kucewicz MT, Cimbalnik J, Matsumoto JY, Brinkmann BH, Bower MR, Vasoli V, Sulc V,
877   Meyer F, Marsh WR, Stead SM, Worrell GA (2014) High frequency oscillations are
878   associated with cognitive processing in human recognition memory. Brain 137:2231–
879   2244.

880   London M, Roth A, Beeren L, Häusser M, Latham PE (2010) Sensitivity to perturbations in vivo
881   implies high noise and suggests rate coding in cortex. Nature 466:123–127.

882   Long NM, Burke JF, Kahana MJ (2014) Subsequent memory effect in intracranial and scalp
883   EEG. NeuroImage 84 Available at:
884   https://www.ncbi.nlm.nih.gov/pmc/articles/PMC3849113/ [Accessed December 5, 2017].

885   Luu P, Tucker DM, Makeig S (2004) Frontal midline theta and the error-related negativity:
886   neurophysiological mechanisms of action regulation. Clin Neurophysiol 115:1821–1835.

887   Maier ME, di Pellegrino G, Steinhauser M (2012) Enhanced error-related negativity on flanker
888   errors: Error expectancy or error significance? Psychophysiology 49:899–908.

889   Mann HB, Whitney DR (1947) On a Test of Whether one of Two Random Variables is
890   Stochastically Larger than the Other. Ann Math Stat 18:50–60.

891   Manning JR, Jacobs J, Fried I, Kahana MJ (2009) Broadband shifts in local field potential power
892   spectra are correlated with single-neuron spiking in humans. J Neurosci Off J Soc
893   Neurosci 29:13613–13620.

894   Mazziotta J et al. (2001) A probabilistic atlas and reference system for the human brain:
895   International Consortium for Brain Mapping (ICBM). Philos Trans R Soc Lond B Biol
896   Sci 356:1293–1322.

897   Milekovic T, Ball T, Schulze-Bonhage A, Aertsen A, Mehring C (2013) Detection of Error
898   Related Neuronal Responses Recorded by Electrocorticography in Humans during
899   Continuous Movements. PLoS ONE 8:e55235.

900   Miller KJ, denNijs M, Shenoy P, Miller JW, Rao RPN, Ojemann JG (2007) Real-time functional
901   brain mapping using electrocorticography. NeuroImage 37:504–507.

902   Miller KJ, Sorensen LB, Ojemann JG, den Nijs M (2009) Power-law scaling in the brain surface
903   electric potential. PLoS Comput Biol 5:e1000609.

904   Moore DS, McCabe GP (1989) Introduction to the practice of statistics. New York, NY, US: W
905   H Freeman/Times Books/ Henry Holt & Co.

906   Muthukumaraswamy S (2013) High-frequency brain activity and muscle artifacts in MEG/EEG:
907   A review and recommendations. Front Hum Neurosci 7 Available at:
908   http://journal.frontiersin.org/article/10.3389/fnhum.2013.00138/abstract [Accessed
909   January 2, 2017].

910 Nieuwenhuis S, Ridderinkhof KR, Blom J, Band GPH, Kok A (2001) Error-related brain
911   potentials are differentially related to awareness of response errors: Evidence from an
912   antisaccade task. Psychophysiology 38:752–760.

913 Nieuwenhuis S, Ridderinkhof KR, Talsma D, Coles MGH, Holroyd CB, Kok A, Molen MW van
914   der (2002) A computational account of altered error processing in older age: Dopamine
915   and the error-related negativity. Cogn Affect Behav Neurosci 2:19–36.

916 Nottage JF, Morrison PD, Williams SCR, Ffytche DH (2013) A Novel Method for Reducing the
917   Effect of Tonic Muscle Activity on the Gamma Band of the Scalp EEG. Brain Topogr
918   26:50–61.

919 Nunez PL, Srinivasan R, Westdorp AF, Wijesinghe RS, Tucker DM, Silberstein RB, Cadusch PJ
920   (1997) EEG coherency: I: statistics, reference electrode, volume conduction, Laplacians,
921   cortical imaging, and interpretation at multiple scales. Electroencephalogr Clin
922   Neurophysiol 103:499–515.

923 Oldfield RC (1971) The assessment and analysis of handedness: The Edinburgh inventory.
924   Neuropsychologia 9:97–113.

925 Pistohl T, Schulze-Bonhage A, Aertsen A, Mehring C, Ball T (2012) Decoding natural grasp
926   types from human ECoG. NeuroImage 59:248–260.

927 Potjans TC, Diesmann M (2014) The Cell-Type Specific Cortical Microcircuit: Relating
928   Structure and Activity in a Full-Scale Spiking Network Model. Cereb Cortex 24:785–806.

929 Ray S, Crone NE, Niebur E, Franaszczuk PJ, Hsiao SS (2008) Neural correlates of high-gamma
930   oscillations (60-200 Hz) in macaque local field potentials and their potential implications
931   in electrocorticography. J Neurosci Off J Soc Neurosci 28:11526–11536.

932 Ridderinkhof KR, Vlugt Y de, Bramlage A, Spaan M, Elton M, Snel J, Band GPH (2002)
933   Alcohol Consumption Impairs Detection of Performance Errors in Mediofrontal Cortex.
934   Science 298:2209–2211.

935 Riesel A, Endrass T, Kaufmann C, Kathmann N (2011) Overactive Error-Related Brain Activity
936   as a Candidate Endophenotype for Obsessive-Compulsive Disorder: Evidence From
937   Unaffected First-Degree Relatives. Am J Psychiatry 168:317–324.

938 Ruchsow M, Herrnberger B, Beschoner P, Grön G, Spitzer M, Kiefer M (2006) Error processing
939   in major depressive disorder: Evidence from event-related potentials. J Psychiatr Res
940   40:37–46.

941 Scheller B, Schneider G, Daunderer M, Kochs EF, Zwissler B (2005) High-frequency
942   Components of Auditory Evoked Potentials Are Detected in Responsive but Not in
943   Unconscious Patients. Anesthesiol J Am Soc Anesthesiol 103:944–950.

944 Sederberg PB, Schulze-Bonhage A, Madsen JR, Bromfield EB, McCarthy DC, Brandt A, Tully
945   MS, Kahana MJ (2007) Hippocampal and Neocortical Gamma Oscillations Predict
946   Memory Formation in Humans. Cereb Cortex 17:1190–1196.

947   Shiels K, Hawk LW (2010) Self-regulation in ADHD: The role of error processing. Clin Psychol
948   Rev 30:951–961.

949   Smith MM, Weaver KE, Grabowski TJ, Rao RPN, Darvas F (2014) Non-invasive detection of
950   high gamma band activity during motor imagery. Front Hum Neurosci 8 Available at:
951   http://journal.frontiersin.org/article/10.3389/fnhum.2014.00817/abstract [Accessed
952   January 31, 2017].

953   Softky WR, Koch C (1993) The highly irregular firing of cortical cells is inconsistent with
954   temporal integration of random EPSPs. J Neurosci Off J Soc Neurosci 13:334–350.

955   Spüler M, Bensch M, Kleih S, Rosenstiel W, Bogdan M, Kübler A (2012) Online use of error-
956   related potentials in healthy users and people with severe motor impairment increases
957   performance of a P300-BCI. Clin Neurophysiol 123:1328–1337.

958   Steinhauser M, Yeung N (2010) Decision Processes in Human Performance Monitoring. J
959   Neurosci 30:15643–15653.

960   Storey JD (2002) A direct approach to false discovery rates. J R Stat Soc Ser B-Stat Methodol
961   64:479–498.

962   Storey JD (2003) The positive false discovery rate: a Bayesian interpretation and the q-value.
963   Ann Stat 31:2013–2035.

964   Szurhaj W, Derambure P (2006) Intracerebral study of gamma oscillations in the human
965   sensorimotor cortex. In: Progress in Brain Research (Neuper C, Klimesch W, eds), pp
966   297–310 Event-Related Dynamics of Brain Oscillations. Elsevier. Available at:
967   http://www.sciencedirect.com/science/article/pii/S007961230659020X.

968   Tadel F, Baillet S, Mosher JC, Pantazis D, Leahy RM (2011) Brainstorm: A User-Friendly
969   Application for MEG/EEG Analysis. Comput Intell Neurosci 2011:e879716.

970   Taylor SF, Stern ER, Gehring WJ (2007) Neural Systems for Error Monitoring: Recent Findings
971   and Theoretical Perspectives. The Neuroscientist 13:160–172.

972   Thomson DJ (1982) Spectrum estimation and harmonic analysis. Proc IEEE 70:1055–1096.

973   Tiesinga PHE, José JV (2000) Robust gamma oscillations in networks of inhibitory hippocampal
974   interneurons. Netw Comput Neural Syst 11:1–23.

975   Tort ABL, Komorowski R, Eichenbaum H, Kopell N (2010) Measuring Phase-Amplitude
976   Coupling Between Neuronal Oscillations of Different Frequencies. J Neurophysiol
977   104:1195–1210.

978   Trujillo LT, Allen JJB (2007) Theta EEG dynamics of the error-related negativity. Clin
979   Neurophysiol 118:645–668.

980   Völker M, Schirrmeister RT, Fiederer LDJ, Burgard W, Ball T (2017) Deep Transfer Learning
981   for Error Decoding from Non-Invasive EEG. ArXiv171009139 Cs Q-Bio Available at:
982   http://arxiv.org/abs/1710.09139.

983   Wang XJ, Buzsáki G (1996) Gamma oscillation by synaptic inhibition in a hippocampal
984   interneuronal network model. J Neurosci Off J Soc Neurosci 16:6402–6413.

985   White JA, Chow CC, Rit J, Soto-Treviño C, Kopell N (1998) Synchronization and Oscillatory
986   Dynamics in Heterogeneous, Mutually Inhibited Neurons. J Comput Neurosci 5:5–16.

987   Whitham EM, Lewis T, Pope KJ, Fitzgibbon SP, Clark CR, Loveless S, DeLosAngeles D,
988   Wallace AK, Broberg M, Willoughby JO (2008) Thinking activates EMG in scalp
989   electrical recordings. Clin Neurophysiol 119:1166–1175.

990   Whitham EM, Pope KJ, Fitzgibbon SP, Lewis T, Clark CR, Loveless S, Broberg M, Wallace A,
991   DeLosAngeles D, Lillie P, Hardy A, Fronsko R, Pulbrook A, Willoughby JO (2007)
992   Scalp electrical recording during paralysis: Quantitative evidence that EEG frequencies
993   above 20 Hz are contaminated by EMG. Clin Neurophysiol 118:1877–1888.

994   Wilson HR, Cowan JD (1972) Excitatory and inhibitory interactions in localized populations of
995   model neurons. Biophys J 12:1–24.

996   Yordanova J, Falkenstein M, Hohnsbein J, Kolev V (2004) Parallel systems of error processing in
997   the brain. NeuroImage 22:590–602.

998   Yuval-Greenberg S, Tomer O, Keren AS, Nelken I, Deouell LY (2008) Transient Induced
999   Gamma-Band Response in EEG as a Manifestation of Miniature Saccades. Neuron
1000   58:429–441.

1001   Zavala B, Brittain J-S, Jenkinson N, Ashkan K, Foltynie T, Limousin P, Zrinzo L, Green AL,
1002   Aziz T, Zaghloul K, Brown P (2013) Subthalamic Nucleus Local Field Potential Activity
1003   during the Eriksen Flanker Task Reveals a Novel Role for Theta Phase during Conflict
1004   Monitoring. J Neurosci 33:14758–14766.

1005

1006 **Tables**

1007 **Table 2: Excerpt of studies about error-related spectral power modulations in EEG & MEG.**

1008 As frequency band definitions were not consistent amongst the publications, the respective definition is

1009 stated within parentheses.

Author / year	Signals	Error-related spectral modulations	Paradigm
Yordanova et al., 2004	64 EEG channels	**Delta (1.5-3.5 Hz)** amplitude increase during ERN/Ne component, **theta (4-8 Hz)** amplitude increase associated with erroneous motor execution.	Four-choice reaction task. 14 subjects (thereof 4 subjects rejected due to too low error rate).
Luu et al., 2004	128 EEG channels	**Theta power (4-7 Hz) increase** at midfrontal channels, starting with response, ending 400ms after ERN/Ne peak.	Forced-choice speeded response paradigm, 11 subjects.
Kolev et al., 2005	64 EEG channels	Error-specific **delta band (1.5-3.5 Hz)** power increase and phase locking. **Theta power (4-7 Hz)** increase after errors in young subjects, not in older subjects.	Four-choice reaction task. 10 "young" subjects (mean age 22.5±1.5 years), 11 "older" subjects (mean age 58.3±2.1 years).
Trujillo and Allen, 2007	25 EEG channels	**Theta power (4-7 Hz) increase** at midfrontocentral sites, 150ms prior to button press until 400ms after it. Stronger increase in non-phase-locked power than in phase-locked power.	Eriksen flanker task, 21 subjects. Stimuli: 'SSSSS', 'HHHHH', 'SSHSS', and 'HHSHH'
Koelewijn et al., 2008	151 MEG sensors	**Beta power (15-35 Hz) depression** during erroneous task execution, then beta rebound	Motor error observation task. Effect sources identified as dorsal motor areas. 12 subjects (9m, 3f).
Carp and Compton, 2009	8 EEG channels	**Alpha power (10-14 Hz)** increase, then decrease in correct trials; absent in erroneous trials.	Stroop task; 81 subjects (46f, 35m).